

Optical polaron formation in quantum systems with permanent dipoles

Adam Burgess,^{1, 2, *} Marian Florescu,^{2, †} and Dominic M. Rouse^{3, 4, ‡}

¹*Leverhulme Quantum Biology Doctoral Training Centre,
University of Surrey, Guildford, GU2 7XH, United Kingdom*

²*Department of Physics and Advanced Technology Institute,
University of Surrey, Guildford, GU2 7XH, United Kingdom*

³*School of Physics and Astronomy, University of Glasgow, Glasgow G12 8QQ, Scotland, United Kingdom*

⁴*Department of Physics and Astronomy, University of Manchester,
Oxford Road, Manchester M13 9PL, United Kingdom*

(Dated: March 8, 2023)

Many optically active systems possess spatially asymmetric electron orbitals. These generate permanent dipole moments, which can be stronger than the corresponding transition dipole moments, significantly affecting the system's dynamics. We introduce a master equation for such systems by employing an optical polaron transformation that captures the photon mode displacements induced by the permanent dipoles and provides an intuitive framework to explore their influence on the system dynamics and emission spectrum. We find that permanent dipoles introduce exciton pumping, multiple photon processes, a photon sideband, and substantial modifications to single-photon transition dipole processes. We derive the emission spectrum of the system, highlighting experimentally detectable signatures of optical polarons, and measurements that can identify the parameters in the system Hamiltonian, the magnitudes of the permanent dipoles, and steady-state populations of the system.

I. INTRODUCTION

In general, the interaction of atomic systems with light is well understood, and the optical master equation describing exciton creation and annihilation through photon emission and absorption, respectively, is derived in many introductory texts dedicated to open quantum systems [1–4]. Atomic systems have highly symmetric electron orbitals and so possess negligible permanent dipoles. However, many physical systems do not share this property and can possess permanent dipoles stronger than their transition dipole moments. Such systems include molecules with parity mixing of the molecular state [5–12], quantum dots with asymmetric confining potentials [13–23], nanorods with non-centrosymmetric crystallographic lattices [24–26], and superconducting circuits [27].

Permanent dipoles introduce additional pure dephasing interactions into the Hamiltonian. The non-additivity of the pure dephasing interaction with the transition dipole interaction yields unique physical effects, including modifications to decoherence [28, 29], steady-state coherence [28, 30, 31], laser-driven population inversion [32], multiphoton conversion [33], entanglement generation [34, 35], and second-harmonic generation [36, 37]. Understanding the role of strong permanent dipoles is highly relevant for the design of new quantum technologies, as well as in exploring novel biochemical processes. Previous studies have either neglected the permanent dipole moments assuming only a pure dephas-

ing interaction [12], have considered single-mode fields [29, 38–40], or have treated the permanent dipoles in a perturbative manner [12, 28, 29, 34, 38–40]. Furthermore, most studies neglect an additional identity interaction also induced by the permanent dipoles, which, as we show here, modifies the initial state of the system and environment and can have a significant impact on the system dynamics. Consequently, such treatments do not capture the role of strong permanent dipoles in asymmetric systems under illumination by multimode fields, such as common thermal fields, which can significantly influence the system's dynamics.

In this paper, we utilise a polaron transformation of the photon modes to derive a master equation valid for systems with strong permanent dipoles. The polaron transformation is a unitary displacement transformation widely used when dealing with strong, pure dephasing interactions. It is typically employed to treat strong vibrational coupling [41–48], and has been crucial in revealing non-additive effects between interactions of light and vibrational excitations [49–51]. In the polaron frame, pure dephasing interactions are absorbed into the definition of the basis and treated to all orders in the coupling strength. We refer to the quasiparticles formed as optical polarons, a mixture of electronic and photonic excitations, to differentiate them from the more common phononic polarons. The optical polaron formalism provides us an essential intuition for the very complex phenomena induced by the permanent dipoles and allows us to unpick their influence on the system dynamics and the features present in the emission spectrum.

In this work, we make no assumptions about the dipole matrix beyond the usual approximation of perturbative *transition* dipole moments. We show that permanent dipoles displace the photon modes, forming optical po-

* a.d.burgess@surrey.ac.uk

† m.florescu@surrey.ac.uk

‡ dominic.rouse@glasgow.ac.uk

larons and resulting in unique physical phenomena such as modifications to single-photon transition dipole processes, entirely new multiple photon processes, the appearance of photonic sidebands, and a permanent-dipole mediated driving between the excited and ground states. We then derive the emission spectrum for the system, highlighting experimentally detectable signatures of the optical polarons.

This paper is organised as follows. In Sec. II, we introduce the Hamiltonian and transform it into the polaron frame, and in Sec. III, we derive the polaron frame master equation and discuss the new physical processes induced by strong permanent dipoles using the analytical expressions. Following this, in Sec. IV, we compare the polaron frame master equation to perturbative dynamics and to numerically exact dynamics using the time-evolving matrix product operators (TEMPO) [51–59] algorithm, using the open source code OQuPy [60]. In Sec. V we derive the emission spectrum, and in Sec. VI, we note two additional points of interest: the roles of the initial conditions and of the dipolar angles on the rates. Finally, we present concluding remarks in Sec. VII.

II. THE MODEL AND POLARON FRAME

We consider the simplest system with permanent dipoles: an asymmetric emitter with a single quantised dipole coupled to a multimode cavity. After truncating the material subsystem to its two lowest energy levels, the fundamental multipolar-gauge Hamiltonian is

$$H = \epsilon\sigma_z + \sum_k \nu_k a_k^\dagger a_k - \mathbf{d} \cdot \mathbf{\Pi}, \quad (1)$$

where ϵ is half the transition energy of the quantum emitter, $\mathbf{\Pi} = -i \sum_k \mathbf{e}_k (a_k^\dagger f_k e^{i\mathbf{k}\cdot\mathbf{r}} - a_k f_k^* e^{-i\mathbf{k}\cdot\mathbf{r}})$ is the electric displacement field, $k = \{\mathbf{k}, \lambda\}$ is a four-vector representing both the wavevector and polarisation state of the mode, and \mathbf{e}_k is the polarisation unit-vector of the mode with energy ν_k and coupling strength f_k with a_k and a_k^\dagger the field mode annihilation and creation operators [61–63]. In the truncated system Hilbert space, the dipole operator is

$$\mathbf{d} = \begin{pmatrix} \mathbf{d}_{ee} & \mathbf{d}_{eg} \\ \mathbf{d}_{ge} & \mathbf{d}_{gg} \end{pmatrix} = \mathbf{d}_\Delta \sigma_z + \mathbf{d}_D \mathcal{I} + \mathbf{d}_\mu \sigma_+ + \mathbf{d}_\mu^* \sigma_-, \quad (2)$$

where the Pauli operators are $\sigma_z = |e\rangle\langle e| - |g\rangle\langle g|$, $\sigma_+ = |e\rangle\langle g|$, $\sigma_- = |g\rangle\langle e|$, $\mathcal{I} = |g\rangle\langle g| + |e\rangle\langle e|$, and $\mathbf{d}_{ij} = \langle i|\mathbf{d}|j\rangle$ for $i, j \in \{e, g\}$. We have defined the following combinations of dipole matrix elements,

$$\mathbf{d}_\Delta = \frac{\mathbf{d}_{ee} - \mathbf{d}_{gg}}{2}, \quad \mathbf{d}_D = \frac{\mathbf{d}_{ee} + \mathbf{d}_{gg}}{2}, \quad \mathbf{d}_\mu = \mathbf{d}_{eg}, \quad (3)$$

which play an essential role in our analysis. Hermiticity of H requires that $\mathbf{d}_{ii} \in \mathbb{R}$ and $\mathbf{d}_{eg} = \mathbf{d}_{ge}^*$. Moreover, the \mathbf{d}_{ij} vectors are not guaranteed to be co-linear.

At this point, it is often assumed that either $|\mathbf{d}_\Delta|, |\mathbf{d}_D| \ll |\mathbf{d}_\mu|$ which leads to the standard optical master equation [1–4], or that $|\mathbf{d}_D| = 0$ and $|\mathbf{d}_\Delta| \gg |\mathbf{d}_\mu|$ leading to a pure dephasing interaction [12]. In this study, we make no assumptions about the size of the permanent dipoles.

Substituting Eq. (2) into Eq. (1) we find that

$$H = \epsilon\sigma_z + \sum_k \nu_k a_k^\dagger a_k + A_{DD} \mathcal{I} + A_{\Delta\Delta} \sigma_z + A_{\mu\bar{\mu}} \sigma_+ + A_{\bar{\mu}\mu} \sigma_-, \quad (4)$$

where

$$A_{pq} = \sum_k (p_k a_k^\dagger + q_k^* a_k), \quad (5)$$

$$p_k = i f_k e^{i\mathbf{k}\cdot\mathbf{r}} (\mathbf{d}_p \cdot \mathbf{e}_k), \quad (6)$$

with $p, q \in \{\mu, \bar{\mu}, D, \Delta\}$ and we denote $d_{\bar{\mu}} = d_\mu^*$. We refer to Eq. (4) as the lab frame Hamiltonian, which is equivalent to Eq. (1).

The photon-only part of Eq. (4) can be diagonalised by the displacement transformation $H_d = B(D/\nu)HB(-D/\nu)$, where subscript d denotes the displaced frame, and displacement operators are given by

$$B(\alpha) = e^{\sum_k (\alpha_k a_k^\dagger - \alpha_k^* a_k)}, \quad (7)$$

and $B(\alpha)^\dagger = B(-\alpha)$. These act on photon operators by

$$B(\pm\alpha) a_k B(\mp\alpha) = a_k \mp \alpha_k, \quad (8)$$

and we further analyse the displacement operators in Appendix A. Ignoring a constant term $-\sum_k |D_k|^2/\nu_k$, the resulting Hamiltonian is $H_d = H_{d,0} + H_{d,I}$ where the unperturbed and interaction Hamiltonians are

$$H_{d,0} = \epsilon' \sigma_z + V \sigma^+ + V^* \sigma^- + \sum_k \nu_k a_k^\dagger a_k, \quad (9a)$$

$$H_{d,I} = A_{\Delta\Delta} \sigma_z + A_{\mu\bar{\mu}} \sigma_+ + A_{\bar{\mu}\mu} \sigma_-, \quad (9b)$$

respectively. Here

$$\epsilon' = \epsilon - \sum_k \frac{D_k \Delta_k^* + D_k^* \Delta_k}{\nu_k}, \quad (10)$$

$$V = - \sum_k \frac{\mu_k D_k^* + \bar{\mu}_k^* D_k}{\nu_k}. \quad (11)$$

Clearly, the permanent dipoles have displaced the photon modes by D_k/ν_k , which results in a renormalised two-level system energy ϵ' and a driving term V .

Throughout this paper, we make the standard assumption that the transition dipole moment \mathbf{d}_μ is small enough to permit an accurate second-order perturbative expansion in its magnitude $|\mathbf{d}_\mu|$. Even for perturbative transition dipole moments, the master equation derived using H in Eq. (4), referred to as the *lab frame master equation* (LFME), will become inaccurate if $|\mathbf{d}_D|g, |\mathbf{d}_\Delta|g \gtrsim 2\epsilon$

where $g = \sqrt{\sum_{\mathbf{k}} |f_{\mathbf{k}}|^2}$ is a measure of the photon coupling strength. The *displaced frame master equation* (DFME), derived from Eq. (9), will similarly breakdown when $|\mathbf{d}_{\Delta}|g$ is comparable to the eigenenergy of the system-only part of $H_{d,0}$.

To overcome this challenge, we make a polaron transformation prior to deriving the Redfield master equation. In this case, the pure dephasing interaction is absorbed into the definition of a new basis which describes an optical polaron quasiparticle. In Fig. 1, we illustrate the various frames introduced and the optical polaron concept. A Redfield master equation derived in the new basis, termed the *polaron frame master equation* (PFME), will be robust to all magnitudes of the permanent dipoles and will recover the DFME in the limit of $\Delta_k \rightarrow 0$, and the LFME when $\Delta_k, D_k \rightarrow 0$.

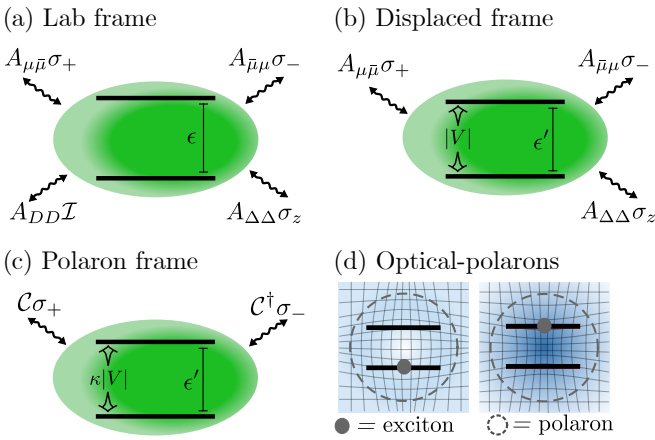


FIG. 1. **Illustration of the model and the optical polaron concept.** (a)-(c) depicts the molecular energies and interactions in the (a) lab frame, (b) displaced frame and (c) polaron frame. (d) is an illustration of an optical polaron: a quasiparticle formed of the exciton and the displaced photon mode.

The polaron frame Hamiltonian is $H_p = U H_d U^\dagger$, where

$$U = B \left(\frac{\Delta}{\nu} \right) |e\rangle \langle e| + B \left(-\frac{\Delta}{\nu} \right) |g\rangle \langle g|. \quad (12)$$

Using Eq. (8), we obtain $H_p = H_{p,0} + H_{p,I}$, where

$$H_{p,0} = \epsilon' \sigma_z + \kappa (V \sigma_+ + V^* \sigma_-) + \sum_k \nu_{\mathbf{k}} a_k^\dagger a_k, \quad (13a)$$

$$H_{p,I} = [C - \kappa V] \sigma_+ + [C^\dagger - \kappa V^*] \sigma_-, \quad (13b)$$

and $\kappa = \langle B(\pm 2\Delta/\nu) \rangle$ with values $0 \leq \kappa \leq 1$, and the coupling operator C is given by

$$C = B \left(\frac{2\Delta}{\nu} \right) \sum_k \left[\mu_k \left(a_k^\dagger + \frac{\Delta_k^* - D_k^*}{\nu_{\mathbf{k}}} \right) + \bar{\mu}_k^* \left(a_k + \frac{\Delta_k - D_k}{\nu_{\mathbf{k}}} \right) \right]. \quad (14)$$

We have ignored a constant term $-\sum_k |\Delta_k|^2/\nu_{\mathbf{k}}$, and have subtracted a term proportional to $\langle C \rangle = \text{Tr}_E(C\rho_E) = \kappa V$ (we show that $\langle C \rangle = \kappa V$ in Appendix B) and its complex conjugate, where

$$\rho_E = \frac{1}{\mathcal{Z}_E} e^{-\beta \sum_k \nu_{\mathbf{k}} a_k^\dagger a_k}, \quad (15)$$

and $\mathcal{Z}_E = \text{Tr}[\exp(-\beta \sum_k \nu_{\mathbf{k}} a_k^\dagger a_k)]$, from the perturbed Hamiltonian and placed it into the unperturbed Hamiltonian such that $\langle H_{p,I} \rangle = 0$. (We denote the partial trace over the photonic environment Hilbert space by $\text{Tr}_E[\cdot]$.) This subtraction is necessary in order to derive a theory that is perturbative about the zero value of the perturbation parameter rather than a finite value.

In the polaron frame Hamiltonian in Eqs. (13), we can now interpret σ_{\pm} as causing transitions between the optical polaron states in Fig. 1(d). Compared to excitons, described by the Hamiltonian in the displaced frame in Eqs. (9), polarons are driven at a weaker amplitude and experience a more complex interaction, albeit one without a pure dephasing term. We also note that the polaron frame Hamiltonian is diagonal when the transition dipoles vanish. Hence, the pure dephasing interaction of the permanent dipoles leads to trivial dynamics if considered in isolation from the transition dipoles.

We now take the continuum limit of the photon modes by introducing the spectral density

$$J(\nu) = \alpha \Theta(\nu) \sum_{\mathbf{k}} |f_{\mathbf{k}}|^2 \delta(\nu - \nu_{\mathbf{k}}), \quad (16)$$

where $\Theta(\nu)$ is the Heaviside step function, and $\alpha = |\mathbf{d}_{\text{ref}}|^2$ where $|\mathbf{d}_{\text{ref}}|$ is a reference magnitude to which we measure other dipole strengths. We include α in Eq. (16) so that $J(\nu)$ has units of energy. This is largely for book-keeping and we quote the dimension-full dipole strengths in our results. In the continuum limit, summations over an arbitrary function $F(\nu)$ transform according to

$$\begin{aligned} & \sum_k |f_{\mathbf{k}}|^2 F(\nu_{\mathbf{k}}) (\mathbf{d}_p \cdot \mathbf{e}_k) (\mathbf{d}_q \cdot \mathbf{e}_k) \\ & \rightarrow \int_0^\infty d\nu J(\nu) F(\nu) \int_{\Omega_{\mathbf{k}}} d\Omega_{\mathbf{k}} \sum_{\lambda} (\tilde{\mathbf{d}}_p \cdot \mathbf{e}_k) (\tilde{\mathbf{d}}_q \cdot \mathbf{e}_k), \end{aligned} \quad (17)$$

where $\tilde{\mathbf{d}}_p = \mathbf{d}_p/|\mathbf{d}_{\text{ref}}|$ and the solid angle integral is $\int_{\Omega_{\mathbf{k}}} d\Omega_{\mathbf{k}} = \int_0^\pi d\theta_{\mathbf{k}} \sin(\theta_{\mathbf{k}}) \int_0^{2\pi} d\phi_{\mathbf{k}}$ [2]. For free space and unpolarised light, we find

$$\begin{aligned} & \int_{\Omega_{\mathbf{k}}} d\Omega_{\mathbf{k}} \sum_{\lambda} (\tilde{\mathbf{d}}_p \cdot \mathbf{e}_k) (\tilde{\mathbf{d}}_q \cdot \mathbf{e}_k) = \frac{8\pi}{3} (\tilde{\mathbf{d}}_p \cdot \tilde{\mathbf{d}}_q) \\ & \equiv \Omega_{pq}, \end{aligned} \quad (18)$$

which is dimensionless. Additionally, in the continuum limit $\kappa = \exp[-\phi(0)/2]$ with the photon propagator de-

fined by

$$\phi(s) = 4\Omega_{\Delta\Delta} \int_0^\infty d\nu \frac{J(\nu)}{\nu^2} \left[\coth\left(\frac{\beta\nu}{2}\right) \cos(\nu s) - i \sin(\nu s) \right], \quad (19)$$

and the displacement induced energy splitting and driving are given by

$$\epsilon' = \epsilon - 2\Omega_{\Delta\Delta}\lambda, \quad (20)$$

$$V = -2\Omega_{\mu D}\lambda, \quad (21)$$

where we have defined the reorganisation energy

$$\lambda = \int_0^\infty d\nu \frac{J(\nu)}{\nu}. \quad (22)$$

Finally, the unperturbed polaron Hamiltonian in Eq. (13a) can be diagonalised using a unitary rotation, $\epsilon'\sigma_z + \kappa(V\sigma_+ + V^*\sigma_-) = \eta\tau_z$, where

$$\eta = \sqrt{\epsilon'^2 + \kappa^2 |V|^2}, \quad (23)$$

$$\tau_z = |+\rangle\langle+| - |-\rangle\langle-|. \quad (24)$$

The eigenbasis relates to the original basis by

$$\begin{pmatrix} |e\rangle \\ |g\rangle \end{pmatrix} = \begin{pmatrix} \cos\left(\frac{\varphi}{2}\right) e^{-i\frac{\theta}{2}} & -\sin\left(\frac{\varphi}{2}\right) e^{-i\frac{\theta}{2}} \\ \sin\left(\frac{\varphi}{2}\right) e^{i\frac{\theta}{2}} & \cos\left(\frac{\varphi}{2}\right) e^{i\frac{\theta}{2}} \end{pmatrix} \begin{pmatrix} |+\rangle \\ |-\rangle \end{pmatrix}, \quad (25)$$

with $\cos(\varphi) = \epsilon'/\eta$, $\sin(\varphi) = \kappa|V|/\eta$, and

$$\theta = \begin{cases} \arctan\left(i\frac{V-V^*}{V+V^*}\right) & \text{if } \Re[V] > 0, \\ -\frac{\pi}{2}\text{sign}(\Im[V]) & \text{if } \Re[V] = 0, \\ \arctan\left(i\frac{V-V^*}{V+V^*}\right) + \pi & \text{if } \Re[V] < 0. \end{cases} \quad (26)$$

In the eigenbasis, the polaron frame Hamiltonian is

$$H_p = \eta\tau_z + \sum_k \nu_k a_k^\dagger a_k + \sum_{\alpha \in \{z, +, -\}} g_\alpha \tau_\alpha, \quad (27)$$

where we have defined $\tau_+ = |+\rangle\langle-|$, $\tau_- = |-\rangle\langle+|$, and the coupling operators

$$g_z = \frac{1}{2} \sin(\varphi) [\mathcal{C}e^{i\theta} + \mathcal{C}^\dagger e^{-i\theta}], \quad (28a)$$

$$g_+ = \left[\cos^2\left(\frac{\varphi}{2}\right) \mathcal{C}e^{i\theta} - \sin^2\left(\frac{\varphi}{2}\right) \mathcal{C}^\dagger e^{-i\theta} \right], \quad (28b)$$

with $g_- = g_+^\dagger$ and $\mathcal{C} = C - \kappa V$.

III. EFFECTS OF STRONG PERMANENT Dipoles

In this section, we derive the secularised PFME, provide a brief analytical review of it, and analyse the population transfer rates, decoherence rate, and Lamb shift

appearing in the master equation, which are given by Fourier transforms of the environment correlation functions (ECFs). This will allow us to analytically explore the role of the permanent dipoles.

Following the analytical discussion of the PFME, we will compare the PFME to the LFME and DFME, and to the numerically exact TEMPO [51–59], which all serve as benchmarks. In the numerical approach, we use the full non-secular Redfield master equations which we derive in Appendix C for all three frames. We emphasise that the non-secular PFME depends only on the ECFs discussed in the main text.

In the eigenbasis, the secularised, time-local, Redfield master equation is

$$\frac{\partial \rho_{++}(t)}{\partial t} = -\gamma_\downarrow \rho_{++}(t) + \gamma_\uparrow \rho_{--}(t), \quad (29a)$$

$$\frac{\partial \rho_{+-}(t)}{\partial t} = -[\gamma_d + 2i\eta] \rho_{+-}(t), \quad (29b)$$

and $(\partial/\partial t)\rho_{--}(t) = -(\partial/\partial t)\rho_{++}(t)$, and $(\partial/\partial t)\rho_{-+}(t) = (\partial/\partial t)\rho_{+-}(t)^\dagger$, where $\rho_{ij}(t) = \langle i|\rho_S(t)|j\rangle$ for $i, j \in \{+, -\}$, and $\rho_S(t) = \text{Tr}_E[\rho(t)]$. The transition and decoherence rates are

$$\gamma_\downarrow = 2\Re[\Gamma_{\mp\mp}(\pm 2\eta)], \quad (30)$$

$$\gamma_d = \frac{1}{2} [\gamma_\uparrow + \gamma_\downarrow] + 4\Re[\Gamma_{zz}(0)], \quad (31)$$

which are written in terms of the Fourier transforms of the ECFs

$$\Gamma_{\alpha\beta}(\omega) = \int_0^\infty ds e^{i\omega s} \langle g_\alpha^\dagger(s) g_\beta(0) \rangle, \quad (32)$$

for $\alpha, \beta \in \{z, +, -\}$ and $g_\alpha(s)$ is the interaction picture form of g_α in Eqs. (28). Finally, the Lamb shifted eigenenergy is

$$2\bar{\eta} = 2\eta + \Im[\Gamma_{--}(2\eta) - \Gamma_{++}(-2\eta)]. \quad (33)$$

The secular master equation in Eqs. (29) describes population transfer from $|+\rangle$ to $|-\rangle$ at decay rate γ_\downarrow , vice-versa at an excitation rate γ_\uparrow , decoherence at a rate γ_d , and oscillations in the coherence at frequency $2\bar{\eta}$.

In the PFME we choose the initial state to be $\rho_p(0) = |g\rangle\langle g| \otimes \rho_E$ where ρ_E is given in Eq. (15) and assume that the environment state does not change. We discuss the implications of this choice for the LFME and DFME at the end of the paper in Sec. VI A.

Evaluating the ECFs in Eq. (32), $\langle g_\alpha^\dagger(s) g_\beta(0) \rangle$, is a laborious process and we present the full derivations in Appendix D. Here, we focus the discussion on new physical processes introduced by the presence of the strong permanent dipoles. The ECFs, $\langle g_\alpha^\dagger(s) g_\beta(0) \rangle$, depend on linear combinations of $\langle \mathcal{C}^\dagger(s) \mathcal{C}(0) \rangle$, $\langle \mathcal{C}(s) \mathcal{C}^\dagger(0) \rangle$, $\langle \mathcal{C}^\dagger(s) \mathcal{C}^\dagger(0) \rangle$ and $\langle \mathcal{C}(s) \mathcal{C}(0) \rangle$, with the relative weighting of each dependent on the sizes of ϵ' and $\kappa|V|$ through the eigenbasis. As proven in Appendix D, each of the two-time correlation functions of $\mathcal{C}(s)$ are the same up to the positions of minus signs and whether the correlation function

scales with only \mathbf{d}_μ , $\mathbf{d}_{\bar{\mu}} = \mathbf{d}_\mu^*$ or a combination, indicating that each describes the same physical processes. For example, we find that

$$\langle \mathcal{C}^\dagger(s)\mathcal{C}(0) \rangle = -\kappa^2 |V|^2 + e^{\phi(s)-\phi(0)} \left[\sum_{n,m=-1}^1 \tilde{A}_{nm}^{(\dagger,\cdot)}(s) + \Omega_{\mu\bar{\mu}} \int_0^\infty d\nu J(\nu) (N(\nu)e^{i\nu s} + \tilde{N}(\nu)e^{-i\nu s}) \right], \quad (34)$$

where $N(\nu) = 1/(e^{\beta\nu} - 1)$, $\tilde{N}(\nu) = 1 + N(\nu)$, and

$$\tilde{A}_{nm}^{(\dagger,\cdot)}(s) = \int_0^\infty d\nu \int_0^\infty d\nu' A_{nm}^{(\dagger,\cdot)}(\nu, \nu') e^{i\nu s} e^{im\nu' s}, \quad (35)$$

is the inverse Fourier transform of $A_{nm}^{(\dagger,\cdot)}(\nu, \nu')$, which we write in matrix notation as

$$A^{(\dagger,\cdot)}(\nu, \nu') = 4 \frac{J(\nu)}{\nu} \frac{J(\nu')}{\nu'} \begin{pmatrix} \Omega_{\bar{\mu}\Delta} \Omega_{\mu\Delta} \tilde{N}(\nu) \tilde{N}(\nu') & -\Omega_{\bar{\mu}\Delta} \Omega_{\mu D} \tilde{N}(\nu) & -\Omega_{\bar{\mu}\Delta} \Omega_{\mu\Delta} \tilde{N}(\nu) N(\nu') \\ -\Omega_{\bar{\mu}D} \Omega_{\mu\Delta} \tilde{N}(\nu') & \Omega_{\bar{\mu}D} \Omega_{\mu D} & \Omega_{\bar{\mu}D} \Omega_{\mu\Delta} N(\nu') \\ -\Omega_{\bar{\mu}\Delta} \Omega_{\mu\Delta} N(\nu) \tilde{N}(\nu') & \Omega_{\bar{\mu}\Delta} \Omega_{\mu D} N(\nu) & \Omega_{\bar{\mu}\Delta} \Omega_{\mu\Delta} N(\nu) N(\nu') \end{pmatrix}, \quad (36)$$

such that, for example, $A_{0,-1}^{(\dagger,\cdot)}(\nu, \nu') = -4[J(\nu)/\nu][J(\nu')/\nu']\Omega_{\bar{\mu}D}\Omega_{\mu\Delta}\tilde{N}(\nu')$. The superscript (\dagger, \cdot) labels the corresponding two-time correlation function of $\mathcal{C}(s)$.

Since the expressions for the remaining three two-time correlation functions of $\mathcal{C}(s)$ are analogous to Eq. (34) up to the appearances of minus signs and the conjugation of transition dipole moments (see Appendix D) we can understand the effects of permanent dipoles considering only Eq. (34). To this end, we now consider the Fourier transform of this two-time correlation function,

$$\Gamma(\omega) = \int_0^\infty ds e^{i\omega s} \langle \mathcal{C}^\dagger(s)\mathcal{C}(0) \rangle. \quad (37)$$

We partition this into three contributions,

$$\Gamma(\omega) = \Gamma_T(\omega) + \Gamma_M(\omega) + \Gamma_{M,SB}(\omega), \quad (38)$$

which we now structure the discussion around.

A. Transition dipole processes, $\Gamma_T(\omega)$

First, we analyse the last term in Eq. (34) proportional to $\Omega_{\mu\bar{\mu}}$, given by

$$\Gamma_T(\omega) = \pi \Omega_{\mu\bar{\mu}} \int_0^\infty d\nu J(\nu) [N(\nu)\mathcal{K}(\omega + \nu) + \tilde{N}(\omega - \nu)\mathcal{K}(\omega - \nu)], \quad (39)$$

where

$$\mathcal{K}(\varepsilon) = \frac{1}{\pi} \int_0^\infty ds e^{i\varepsilon s} e^{\phi(s)-\phi(0)}, \quad (40)$$

contains the influence of the permanent dipoles within this term. The subscript ‘ T ’ identifies that this term

describes processes generated by transition dipoles, since it vanishes if $|\mathbf{d}_\mu| = 0$ but does not vanish if only the permanent dipoles are zero.

To understand the physical processes associated with this term, it is convenient to temporarily ignore the factor of $\exp[\phi(s) - \phi(0)]$. The resulting term is the typical correlation function appearing in the standard optical master equation (SOME) in the absence of permanent dipoles [4],

$$\Gamma_{\text{SOME}}(\omega) = \Omega_{\mu\bar{\mu}} \left[\pi \left(J(-\omega)N(-\omega) + J(\omega)\tilde{N}(\omega) \right) + i\mathcal{P} \int_0^\infty d\nu J(\nu) \left(\frac{N(\nu)}{\omega + \nu} + \frac{\tilde{N}(\nu)}{\omega - \nu} \right) \right], \quad (41)$$

where \mathcal{P} denotes the principal value. Clearly, when $\omega = -2\eta$ the real part of $\Gamma_{\text{SOME}}(\omega)$ describes excitation-by-absorption at a rate $2\pi\Omega_{\mu\bar{\mu}}J(2\eta)N(2\eta)$, and when $\omega = 2\eta$ it describes decay-by-emission at a rate $2\pi\Omega_{\mu\bar{\mu}}J(2\eta)\tilde{N}(2\eta)$. The imaginary part of $\Gamma_{\text{SOME}}(\omega)$ gives the Lamb shift.

We now return to Eq. (39). In Ref. [49] an analytic solution to Eq. (40) was found by exploiting the fact that $\mathcal{K}(\varepsilon)$ only depends on $J(\nu)$ through its moments $\mu_m = 4\Omega_{\Delta\Delta} \int_0^\infty d\nu [J(\nu)/\nu^2]\nu^m$ for $m = 1, 2, \dots, \infty$, and that moments of lower order contribute relatively more. We can then evaluate $\mathcal{K}(\varepsilon)$ by replacing $J(\nu)$ with a truncated spectral density $J'(\nu) = \sum_{\mathbf{k}=1}^{N_*} |f'_\mathbf{k}|^2 \delta(\nu - \nu'_\mathbf{k})$, as long as we choose the coupling strengths $\{f'_\mathbf{k}\}$ and energies $\{\nu'_\mathbf{k}\}$ of the modes such that $J'(\nu)/\nu^2$ has the same lowest moments as μ_m for $m = 1, 2, \dots, 2N_*$ [49]. The solution converges rapidly for increasing N_* , and a single-mode truncation is often very accurate, with truncation mode parameters: $\nu'_1 \equiv \nu_s = \mu_2/\mu_1$ and $f'_1 \equiv f_s = \mu_2^{1/2} \propto \Omega_{\Delta\Delta}^{1/2}$ [49]. A single-mode truncation

captures all of the essential physics described by $\mathcal{K}(\omega)$. Thus, for the analytical analysis in this work, we use a single-mode truncation in the evaluation of Eq. (40); however, in all of the simulations in this paper, we increase N_* until convergence.

From Ref. [49], the single mode solution of Eq. (40) is

$$\mathcal{K}(\varepsilon) = \sum_{\ell=-\infty}^{\infty} A_{\ell} \left[\delta(\varepsilon - \ell\nu_s) + \frac{i}{\pi} \frac{\mathcal{P}}{\varepsilon - \ell\nu_s} \right], \quad (42)$$

where

$$A_{\ell} = \sum_{n=|\ell|}^{\infty'} \sum_{m=\frac{n-\ell}{2}}^n \binom{n}{m} \binom{m}{m - \frac{n-\ell}{2}} W_n V_m, \quad (43)$$

and the prime on the first summation indicates that only every other term is included $n = |\ell|, |\ell| + 2, \dots$, and $W_n = S_s^n \exp[-S_s]/n!$ is the Franck-Condon factor of the mode in the truncation, $S_s = |f_s|^2/\nu_s^2 = \mu_1^2/\mu_2$ is its Huang-Rhys factor and $V_m = N(\nu_s)^m \exp[-2S_s N(\nu_s)]$ [49]. A_{ℓ} has the normalisation property $\sum_{\ell=-\infty}^{\infty} A_{\ell} = 1$, is maximised for $\ell = \text{Round}(S')$, becomes $A_{\ell} = \delta_{\ell 0}$ if $|\mathbf{d}_{\Delta}| = 0$, and the $\ell < 0$ terms are only non-zero at finite temperature (see Ref. [49] for a full discussion on the mode truncation solution).

Substituting Eq. (42) into Eq. (39) yields

$$\Gamma_T(\omega) = \frac{1}{2} \gamma_T(\omega) + iS_T(\omega), \quad (44)$$

where

$$\gamma_T(\omega) = 2\pi\Omega_{\mu\bar{\mu}} \sum_{\ell=-\infty}^{\infty} A_{\ell} \left[J(\ell\nu_s - \omega) N(\ell\nu_s - \omega) + J(\omega - \ell\nu_s) \tilde{N}(\omega - \ell\nu_s) \right], \quad (45)$$

and

$$S_T(\omega) = i\Omega_{\mu\bar{\mu}} \sum_{\ell=-\infty}^{\infty} A_{\ell} \mathcal{P} \int_0^{\infty} d\nu J(\nu) \times \left(\frac{N(\nu)}{\omega + \nu - \ell\nu_s} + \frac{\tilde{N}(\nu)}{\omega - \nu - \ell\nu_s} \right). \quad (46)$$

Eqs. (45) and (46) show that the effect of the permanent dipoles within $\Gamma_T(\omega)$ is to introduce a manifold of harmonic levels (in the single mode truncation of $\mathcal{K}(\varepsilon)$ this results in a single manifold) to/from which transitions can occur, and which influence the Lamb shift value. This is commonly observed when vibrational displacement interactions occur simultaneously with transition dipole interactions and manifest in spectra as vibrational side bands and Stokes's shift. However, in our model, this is a purely photonic effect and it results in a photon sideband in the spectrum of the system. $\Gamma_{\text{SOME}}(\omega)$ in Eq. (41) is recovered from $\Gamma_T(\omega)$ in the limit of no permanent dipoles because $A_{\ell} \rightarrow \delta_{\ell 0}$.

In Fig. 2, we illustrate decay-by-emission transitions corresponding to $\ell = 1$, and decay-by-absorption transitions for $\ell = \ell_*$ where $\text{Round}(2\eta/\nu_s) < \ell_* < \text{Round}(2\eta/\nu_s) + 1$. The A_{ℓ} values can be interpreted as the probabilities for a decay between levels with energy difference $2\eta - \ell\nu_s$ to occur.

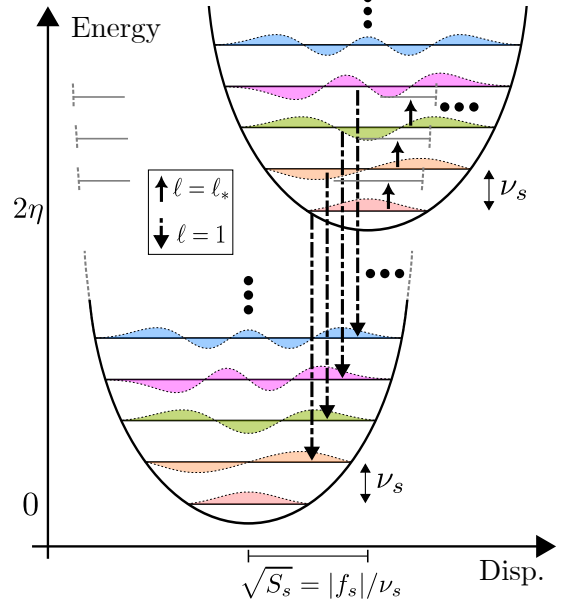


FIG. 2. **Illustration of decay processes** ($\omega = +2\eta$) captured by the $\ell = 1$ and $\ell = \ell_*$ terms in Eq. (45), within the single mode truncation of $\mathcal{K}(\varepsilon)$. Decay-by-emission processes have dot-dashed arrows, and decay-by-absorption processes have solid arrows. The type of decay that occurs for a given value of ℓ depends on the sign of $2\eta - \ell\nu_s$. In the absence of permanent dipoles $A_{\ell} = \delta_{\ell 0}$ and so only the $\ell = 0$ decay process between the two ground harmonic levels in each manifold is possible.

B. Mixed dipole processes, $\Gamma_M(\omega)$ and $\Gamma_{M,\text{SB}}(\omega)$

We now turn our attention to the processes that are wholly associated with the presence of the permanent dipoles, described by the $-\kappa^2|V|^2$ and $\tilde{A}_{nm}^{(\dagger,\cdot)}$ terms in Eq. (34), with the coefficients in Eq. (36). All of these terms vanish if $|\mathbf{d}_{\mu}| = 0$ or $|\mathbf{d}_{\Delta}| = |\mathbf{d}_D| = 0$, and some terms vanish if either $|\mathbf{d}_D|$ or $|\mathbf{d}_{\Delta}|$ are zero with finite $|\mathbf{d}_{\mu}|$. Therefore, we refer to these as mixed dipole processes, denoted by a subscript ‘M’.

The term depending on $\tilde{A}_{nm}^{(\dagger,\cdot)}(s)$ involves the two-frequency Fourier transform in Eq. (35), indicating that two simultaneous processes occur. From the phase factors in Eq. (35), when n or m indices are equal to -1 we deal with emission processes, when they are equal to 0 we have non-radiative processes, and when they are equal to $+1$ we are dealing with absorption, into the frequency channel ν and ν' , respectively. This interpretation is reinforced by the positions of the factors of

$N(\nu)$, $N(\nu')$, $\tilde{N}(\nu)$ and $\tilde{N}(\nu')$ in the matrix in Eq. (36). This matrix also identifies that radiative processes scale as $\Omega_{\mu\Delta} = (8\pi/3)\tilde{\mathbf{d}}_\mu \cdot \tilde{\mathbf{d}}_\Delta$ whilst non-radiative processes scale as $\Omega_{\mu D} = (8\pi/3)\tilde{\mathbf{d}}_\mu \cdot \tilde{\mathbf{d}}_D$ (recall here that whether the scaling is with \mathbf{d}_μ or \mathbf{d}_μ is unimportant but depends on which two-time correlation function of $\mathcal{C}(s)$ is being discussed.) Therefore, the physical processes resulting from permanent dipoles differ depending on whether Δ_k or D_k are large. Finally, Eq. (36) shows that a modified spectral density is relevant for these new processes, namely $J(\nu)/\nu$.

This interpretation, that the $\tilde{A}_{nm}^{(\dagger,\cdot)}(s)$ term describes two-simultaneous processes of either 0 or 1 photon processes, does not take the factor of $\exp[\phi(s) - \phi(0)]$ in Eq. (34) into account. Similar to the case of the transition dipole processes, this factor will introduce a photon sideband to each process.

If n and m are not both equal to zero, then the Fourier transform of the two-time correlation function in Eq. (37) is well-defined and can be performed numerically. We denote these terms as

$$\Gamma_M(\omega) = \kappa^2 \sum_{\substack{n,m=-1 \\ n \neq m}}^1 \int_0^\infty ds e^{i\omega s + \phi(s)} \tilde{A}_{nm}^{(\dagger,\cdot)}(s). \quad (47)$$

The Fourier transforms of the term with $n = m = 0$ (which describes two simultaneous non-radiative processes) and the term $-\kappa^2|V|^2$ (describing the non-zero equilibrium value of C) appear to be either divergent or ill-defined. The former is because $\phi(\infty) = 0$, and so the integrand tends to a finite value at large s , and the latter is due to the lack of s -dependence. But, these problematic terms cancel identically, leaving only

$$\Gamma_{M,SB}(\omega) = \kappa^2|V|^2 \int_0^\infty ds e^{i\omega s} (e^{\phi(s)} - 1). \quad (48)$$

The subscript ‘ M, SB ’ in the equation above denotes that this rate is associated with a mixed dipole process and is generated entirely by the photon sideband. This is highlighted by the factor of $\exp[\phi(s)] - 1$ which vanishes if $|\mathbf{d}_\Delta| = 0$, indicating that $\Gamma_{M,SB}(\omega)$ describes radiative processes despite corresponding to $n = m = 0$. In deriving Eq. (48) we have used that $\tilde{A}_{00}^{(\dagger,\cdot)}(s) = |V|^2$ which is easily verified from Eqs. (35), (36) and (21), which leads to the cancellation of the $-\kappa^2|V|^2$ term in Eq. (34).

In Fig. 3(a) we plot the decay rate γ_\downarrow as a function of $|\mathbf{d}_\Delta|$ for different values of $|\mathbf{d}_D|$, and in Fig. 3(b) we show how the various physical processes contribute to the overall decay rate. The excitation γ_\uparrow and decoherence γ_d rates can be obtained from Fig. 3 by scaling the curves by 0.135 and 0.568, respectively; all three rates have the same dependence on the permanent dipoles unless $|\mathbf{d}_D|$ is ultra-strong ($\sim 5 \text{ eV}^{-1}$ for the parameters in Fig. 3, see Appendix F). The key points resulting from the analysis of Fig. 3 are: (1) one can both increase and decrease rates through the physical mechanisms enabled by the presence of permanent dipoles; (2) all physical processes

found in the polaron ECFs contribute non-negligibly to the total rates, and; (3) the phase of the transition dipole moment is irrelevant to dynamics. Note that in Fig. 3 we alter ϵ when changing other parameters such that ϵ' in Eq. (13) remains constant.

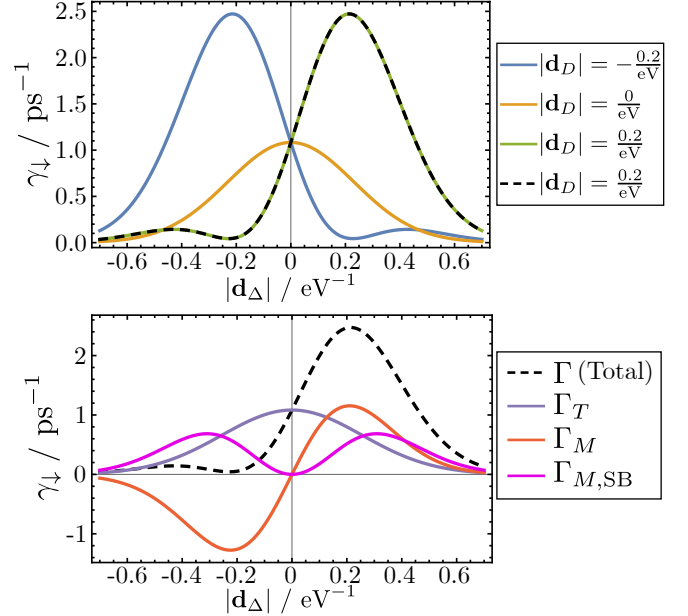


FIG. 3. Polaron frame decay rate for different permanent dipole strengths. (a) shows the decay rate γ_\downarrow as a function of $|\mathbf{d}_\Delta|$ for $|\mathbf{d}_D| = -0.2, 0, 0.2 \text{ eV}^{-1}$. (All dipole matrix elements are co-linear, and we denote a vector with a negative magnitude, e.g. $|\mathbf{d}_\Delta| < 0$, as meaning it is anti-parallel to a vector of positive magnitude.) The solid curves all have $\mathbf{d}_\mu = \mathbf{d}$ with $|\mathbf{d}| = 0.01 \text{ eV}^{-1}$ whilst the dashed black line has $\mathbf{d}_\mu = \mathbf{d}_1 + i\mathbf{d}_2$ where \mathbf{d}_1 and \mathbf{d}_2 are parallel with $|\mathbf{d}_1| = 0.002 \text{ eV}^{-1}$ and \mathbf{d}_2 such that $|\mathbf{d}_\mu| = |\mathbf{d}|$. The agreement of the green and dashed black curves emphasises that the rates do not depend on the phase of \mathbf{d}_μ which is true for all parameter regimes. (b) shows the contributions of the different physical processes to the decay rate for $|\mathbf{d}_D| = 0.2 \text{ eV}^{-1}$. The purple curve is the contribution of transition dipole processes $\Gamma_T(\omega)$ in Eq. (39), the orange curve is the contribution from the mixed dipole processes $\Gamma_M(\omega)$ in Eq. (48), and the magenta curve is the contribution from the sideband-only mixed dipole processes $\Gamma_{M,SB}$ in Eq. (48). The dashed black curve in both panels are the same and corresponds to the total decay rate in Eq. (38). Other parameters in (a) and (b): $\epsilon' = 0.5 \text{ eV}$, $\beta = 2 \text{ eV}^{-1}$ ($T \approx 5800 \text{ K}$), $J(\nu) = \alpha(1/\pi)\Theta(\nu)\nu^3 \exp(-\nu/\nu_c)$ with $\alpha = |\mathbf{d}_{\text{ref}}|^2 = 1 \text{ eV}^{-2}$ and $\nu_c = 1 \text{ eV}$.

IV. COMPARISON TO EXACT DYNAMICS

In this section, we compare the predictions for the system density operator found with the PFME to those with the DFME and LFME, and a numerically exact approach, TEMPO. The perturbative master equations do not capture many of the unique processes attributed to the permanent dipoles as seen in the polaron frame, and

we expect these perturbative approaches to become inaccurate when $|\tilde{\mathbf{d}}_\Delta|\tilde{g}, |\tilde{\mathbf{d}}_D|\tilde{g} \gtrsim 2\eta$ where $\tilde{g} = [\int_0^\infty d\nu J(\nu)]^{0.5}$ is a measure of the mode coupling strength. This is indeed manifest in Fig. 4 where we plot the population of the ground state and the coherence between the excited and ground state against time. We note in the comparison provided in Fig. 4, the PFME provides the most accurate master equation, followed by the DFME, and then the LFME.

The PFME predicts qualitatively correct dynamics and agrees well with TEMPO, even for strong permanent dipoles. In Fig. 4 (a) and (b) $2\eta \approx 0.36$ eV and in (c) and (d) $2\eta = 1$ eV which should be compared to the permanent dipole strengths, which are $|\mathbf{d}_D| = 0.5$ eV $^{-1}$ = $|\mathbf{d}_\Delta|$ in (a) and (b), and $|\mathbf{d}_D| = 0$ eV $^{-1}$ and $|\mathbf{d}_\Delta| = 1$ eV $^{-1}$ in (c) and (d), and $\tilde{g} = \sqrt{6/\pi}$ in all subfigures. This emphasises that each new process in Fig. 3 is required to correctly describe strong permanent dipoles. In subfigures (c) and (d), the LFME and DFME are identical because $|\mathbf{d}_D| = 0$ eV $^{-1}$.

A phenomenon not captured by the PFME or any Markovian master equation is the so-called ‘slip’ [64] at short times, which is most evident in subfigure (d). However, we note that past short times, the PFME and TEMPO both predict the same features in subfigure (d), including the static coherences. Moreover, the PFME predicts the coherences in subfigure (b) accurately, with only a very slight discrepancy in the oscillation period and decoherence rate.

V. EMISSION SPECTRUM

Due to the many new physical processes generated by the presence of permanent dipoles discussed in Sec. III we expect significant alterations to the emission spectrum. In the absence of permanent dipoles, the spectrum should consist of a single peak at the splitting 2ϵ (assuming negligible Lamb shift) with a width determined by the decoherence rate in the standard optical master equation: $\pi J(2\epsilon)[1 + 2N(2\epsilon)]$.

In the presence of permanent dipoles, We expect four major deviations from this picture which can be employed as experimental signatures: (1) the main emission peak will shift from 2ϵ to $2\bar{\eta}$ given in Eq. (33); (2) the width of the main peak will be proportional to γ_d , where γ_d is given in Eq. (31); (3) there will be a photonic sideband with Stokes shift equal to $\mu_1 = 4\Omega_{\Delta\Delta}\lambda$ where λ is given in Eq. (22); and (4) the appearance of a Mollow triplet associated with the exciton driving, $V \propto \Omega_{\mu D}$.

As shown in Appendix G, the emission spectrum is given by

$$I(\omega) = \alpha_{\text{prop}}(\mathbf{r}, \mathbf{R}, \omega) I_0(\omega), \quad (49)$$

where $\alpha_{\text{prop}}(\mathbf{r}, \mathbf{R}, \omega) = |\mathbf{d}_\mu \cdot \mathbf{G}(\mathbf{r}, \mathbf{R}, \omega)|^2$ and $\mathbf{G}(\mathbf{r}, \mathbf{R}, \omega)$ is the Green’s function of the medium [50, 65–68]. $\alpha_{\text{prop}}(\mathbf{r}, \mathbf{R}, \omega)$ accounts for propagation and filtering of

the light from the molecule to the detector at positions \mathbf{r} and \mathbf{R} , respectively [65]. The polarisation spectrum is

$$I_0(\omega) = \langle \sigma^+(\omega) \sigma^-(\omega) \rangle, \quad (50)$$

or, equivalently,

$$I_0(\omega) = \lim_{t \rightarrow \infty} \Re \left[\int_0^\infty d\tau \langle \sigma_+(t + \tau) \sigma_-(t) \rangle e^{-i\omega\tau} \right]. \quad (51)$$

In the following, we focus on evaluating the polarisation spectrum, which captures entirely the effects associated with the permanent dipoles. The specifics of the experimental set-up, for example, whether the molecule is coupled to a cavity or a waveguide, are described by the $\alpha_{\text{prop}}(\mathbf{r}, \mathbf{R}, \omega)$ term, which can be calculated separately.

The expectation value in Eq. (51) is taken with respect to the lab frame density operator ρ . Using $\rho = U^\dagger \rho_p U$ where U is the polaron transformation in Eq. (12) and ρ_p is the polaron frame density operator, we have

$$\begin{aligned} \langle \sigma_+(t + \tau) \sigma_-(t) \rangle &= \kappa^2 e^{\phi(\tau)} \text{Tr} [\sigma_+(t + \tau) \sigma_-(t) \rho_p(0)] \\ &\equiv \kappa^2 e^{\phi(\tau)} \langle \sigma_+(t + \tau) \sigma_-(t) \rangle_p. \end{aligned} \quad (52)$$

Therefore, the final expression for the polaron frame polarisation spectrum is

$$\begin{aligned} I_{p,0}(\omega) &= \kappa^2 \lim_{t \rightarrow \infty} \Re \left[\int_0^\infty d\tau e^{\phi(\tau)} \right. \\ &\quad \left. \times \langle \sigma_+(t + \tau) \sigma_-(t) \rangle_p e^{-i\omega\tau} \right]. \end{aligned} \quad (53)$$

The two-time correlation function in Eq. (53) can be calculated using the quantum regression theorem (QRT) [1, 69]. The QRT utilises the cyclicity of the trace to rewrite the two-time expectation value as

$$\lim_{t \rightarrow \infty} \langle \sigma_+(t + \tau) \sigma_-(t) \rangle_p = \text{Tr} [\sigma^+ \Lambda_p(\tau)], \quad (54)$$

where $\Lambda_p(\tau) = U_0^\dagger(\tau) \Lambda_p(0) U_0(\tau)$ is a modified density operator with the initial state

$$\Lambda_p(0) = \sigma^- U_0(\infty) \rho_p(0) U_0^\dagger(\infty), \quad (55)$$

and, because $U_0(\tau)$ is the time evolution operator defined by the polaron frame Hamiltonian (see Eq. (13)), the master equation we have derived holds identically for the $\Lambda_p(\tau)$ operator but with the initial condition defined by Eq. (55). The QRT allows one to convert two-time correlation functions into one-time expectation values of density operators with modified initial conditions.

Due to the polaron transformation, Eq. (53) captures the photonic sideband. However, the QRT contains an implicit Born approximation [69] as well as any approximations used in the evaluation of the master equation.

Owing to the modified initial state in Eq. (55), the power of the polarisation spectrum contains information about the steady state of the system,

$$P = \int_{-\infty}^\infty d\omega I_{p,0}(\omega) = \pi \rho_{ee}(\infty). \quad (56)$$

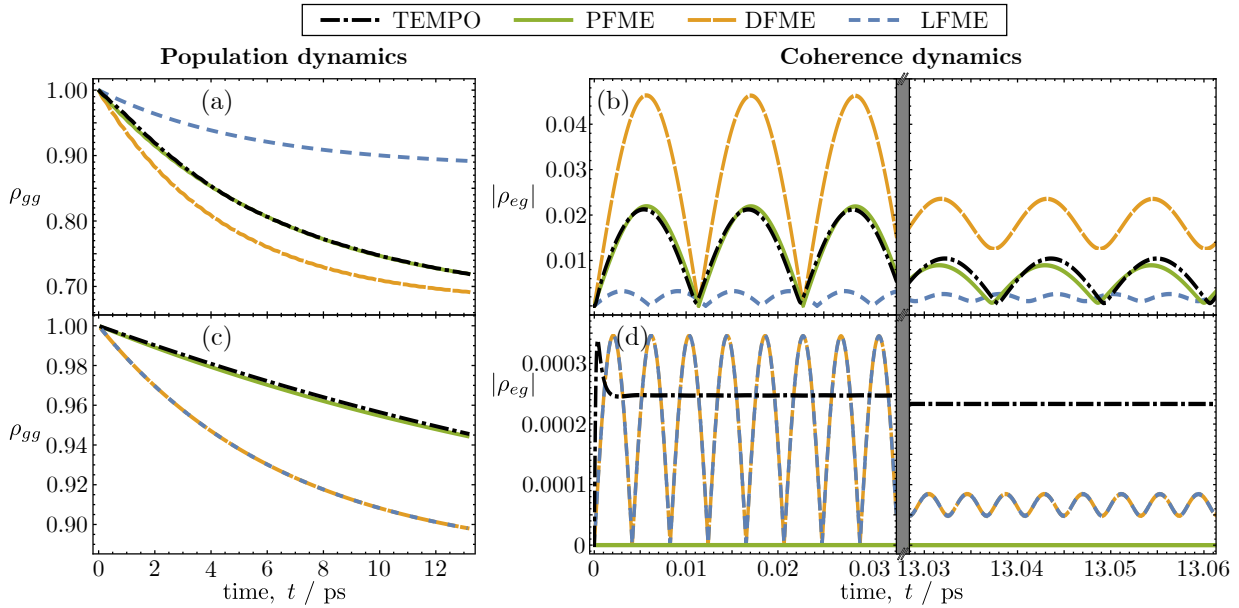


FIG. 4. **Comparison of the PFME predictions to exact numerical approach and perturbative master equations.** (a) and (c) are a comparison of $\rho_{gg}(t)$ calculated using the PFME (green) to TEMPO (dot-dashed black), the LFME (short-dashed blue), and the DFME (long-dashed orange) over short and long times. (b) and (d) A similar comparison but now for $|\rho_{eg}(t)|$ (note the discontinuity in the time axis). For (a) and (b), $|\mathbf{d}_D| = 0.5 \text{ eV}^{-1} = |\mathbf{d}_\Delta|$, while for (c) and (d) $|\mathbf{d}_D| = 0 \text{ eV}^{-1}$ and $|\mathbf{d}_\Delta| = 1 \text{ eV}^{-1}$. Other parameters are the same as in Fig. 3, except that here $\epsilon = 0.5 \text{ eV}$ (instead of ϵ'). To make comparison to TEMPO easier, we have assumed that the field aligns with the dipole moments, such that all dipoles are parallel or anti-parallel and we have ignored the factor of $8\pi/3$ in Eq. (18).

Additionally, by noting that the polarisation spectrum without the photon sideband, denoted by $I_{p,\times}(\omega)$, is given by Eq. (53) with the replacement $\exp[\phi(\tau)] \rightarrow 1$, one can show that

$$\frac{\int_{-\infty}^{\infty} d\omega I_{p,\times}(\omega)}{P} = \kappa^2. \quad (57)$$

Remarkably, an integrated spectrum measurement can be used to determine κ , which in turn provides an effective measurement of $\Omega_{\Delta\Delta}$ and, therefore, of the strength of the $|\mathbf{d}_\Delta|$ dipole moment. In measurements, $I_{p,\times}(\omega)$ cannot be separated from $I_{p,0}(\omega)$, but as we show in the following, $\int_{-\infty}^{\infty} d\omega I_{p,\times}(\omega)$ can be accurately approximated as the integral of the measured spectrum over the Lorentzian parts of the dominant peaks [70].

In Fig. 5, we plot the polarisation spectrum calculated in the polaron frame $[I_{p,0}(\omega)]$ in dot-dashed green, in blue we plot the spectrum for the same parameters but without the photonic sideband $[I_{p,\times}(\omega)]$ which serves to highlight the sideband, and in dotted orange we plot the polarisation spectrum in the absence of permanent dipoles $[I_{p,npd}(\omega)]$. In subfigure (a) $|\mathbf{d}_D| = |\mathbf{d}_\Delta| = 0.05 \text{ eV}^{-1}$, (b) $|\mathbf{d}_D| = 0.5 \text{ eV}^{-1}$ and $|\mathbf{d}_\Delta| = 0.08 \text{ eV}^{-1}$, and all other parameters are the same in both subfigures and given in the caption of Fig. 3. The insets show zoom-ins of the dominant peaks, and the vertical solid black line indicates the Lamb shifted eigenfrequency $\pm 2\bar{\eta}$ given in Eq. (33) whilst the dashed black vertical line is at 2ϵ where the spectrum peaks in the absence of permanent dipoles. The

four signatures of permanent dipoles are evident: different position and width of the zero photon line, a photon sideband, a zero frequency peak at small $|\mathbf{d}_D|$ which becomes the central peak in the Mollow triplet at large $|\mathbf{d}_D|$.

In Fig. 5(a), a peak extending to negative (unphysical) values can be seen at $\omega = -2\bar{\eta}$. This originates from the non-secular rate that couples the coherences $\rho_{+-}(t)$ and $\rho_{-+}(t)$. This unphysical peak also occurs in the SOME, where the relevant non-secular rate arises from the counter-rotating terms in the interaction Hamiltonian. There, its amplitude scales as $-E_L^2$, where E_L is the Lamb shift, which is negligible for perturbative transition dipoles. At the larger value of $|\mathbf{d}_D|$ in Fig. 5(b), this peak inverts and the three peaks at $\omega = \{-2\bar{\eta}, 0, 2\bar{\eta}\}$ form a Mollow triplet.

We now introduce a procedure of directly obtaining essential information about the system from the experimentally measurable spectrum, $I_{p,0}(\omega)$, and compare the values obtained for the data shown in Fig. 5 to analytic values. We show that it is possible to evaluate κ and $\rho_{ee}(\infty)$ from $I_{p,0}(\omega)$ using Eqs. (56) and (57) and, provided that the temperature of the experiment is known, these values can be used to obtain ϵ' and $|V|$. If the spectral density is also known, it is then possible to obtain $|\mathbf{d}_\Delta|$ and a lower bound for one of $|\mathbf{d}_D|$ or $|\mathbf{d}_\mu|$. The lower bound becomes an equality if \mathbf{d}_D and \mathbf{d}_μ are co-linear. We note that information about the orientation of dipole moments or the phase of V is not attainable through the

spectrum. The values of the parameters obtained from the spectrum (methods explained afterwards) and the analytic values are given in Table I.

Param.	Analytic (a)	Meas. (a)	Analytic (b)	Meas. (b)
κ^2	0.9616	0.9616	0.9047	0.9088
$\rho_{ee}(\infty)$	0.13088	0.13090	0.4275	0.4467
ϵ'/eV	0.4733	0.4732	0.0733	0.0749
$ V /\text{eV}$	0.0052	N/A	0.0533	0.0498
$ \mathbf{d}_\Delta /\text{eV}^{-1}$	0.0500	0.0500	0.0800	0.0802
$ \mathbf{d}_D /\text{eV}^{-1}$	0.0500	N/A	0.500	0.501

TABLE I. **Values of parameters obtainable from the measurable spectrum.** Each column shows analytic values, obtained directly from the equations in this paper, and ‘measured’ values obtained from $I_{p,0}(\omega)$ in Fig 5. The left-hand column is for Fig. 5(a) and the right-hand column for Fig. 5(b). ‘N/A’ in the ‘Meas. (a)’ column indicates that $|V|$ could not be obtained from the spectrum because it is of comparable magnitude to the Lamb shifts. We have assumed that $|\mathbf{d}_\mu|$ is known allowing $|\mathbf{d}_D|$ to be calculated for from $|V|$ in (b). This is an equality instead of a lower bound since \mathbf{d}_D and \mathbf{d}_μ are parallel in Fig. 5.

As shown in Eq. (56), the steady state population of the excited state can straightforwardly be obtained by integrating $I_{p,0}(\omega)$ over all frequencies. κ can be approximately found using Eq. (57) with $\int_{-\infty}^{\infty} d\omega I_{p,\times}(\omega) \approx \int_R d\omega I_{p,0}(\omega)$ where R are the frequency regions for which the dominant peaks in the spectrum are approximately Lorentzian before the photon sideband begins. These regions are shown by the shaded regions in the insets of Fig. 5. One can then estimate the remaining parameters of the system by assuming that the system thermalises with respect to $H_{p,0}$ in Eq. (13a), yielding the steady state

$$\rho_{ee}(\infty) = \frac{1}{2} \left[1 - \frac{\epsilon'}{\eta} \tanh(\beta\eta) \right]. \quad (58)$$

Using Eq. (58), assuming negligible Lamb shifts so that one may take 2η as the peak position of the positive frequency peak of $I_{p,0}(\omega)$, an estimation for ϵ' can be obtained, and subsequently for $|V|$ using Eq. (23). If the spectral density of the photon bath is known, one can invert the relation $\kappa = \exp[-\phi(0)/2]$ to obtain $|\mathbf{d}_\Delta|$. Finally, if one of $|\mathbf{d}_D|$ or $|\mathbf{d}_\mu|$ is known, then a lower bound for the magnitude of the unknown dipole moment can be found using Eq. (11).

VI. DISCUSSION

A. Importance of initial conditions

It is typical in theoretical quantum optics to consider the system and environment initially in an uncorrelated state,

$$\rho(0) = \rho_S(0) \otimes \rho_E, \quad (59)$$

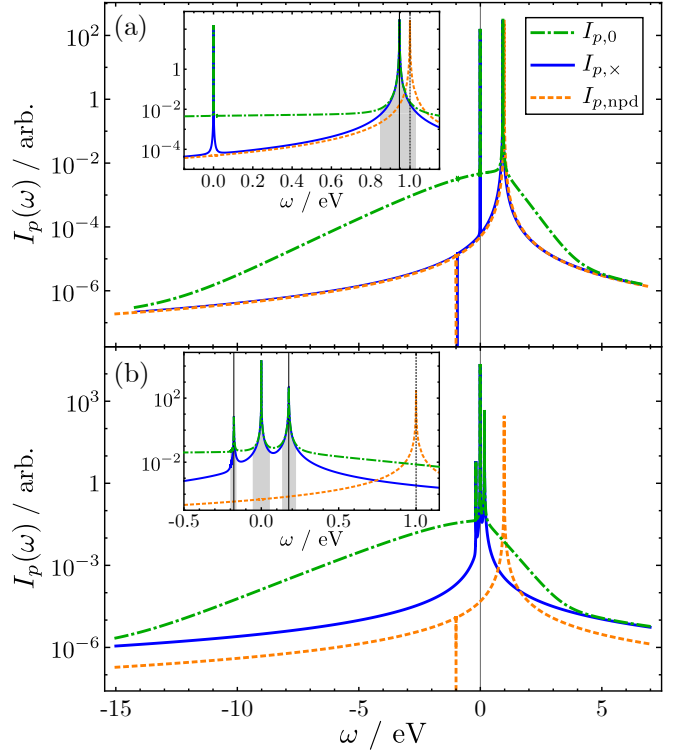


FIG. 5. **Polarisation spectrum of the system.** The total polarisation $I_{p,0}(\omega)$ is shown in dot-dashed green, the polarisation spectrum without the photon sideband $I_{p,\times}(\omega)$ in solid blue, and the polarisation spectrum with $|\mathbf{d}_\Delta| = |\mathbf{d}_D| = 0$ (and other parameters unchanged) $I_{p,npd}(\omega)$ is shown in dotted orange. In all curves $\epsilon = 0.5 \text{ eV}^{-1}$, and in $I_{p,0}(\omega)$ and $I_{p,\times}(\omega)$ we use co-linear dipoles with $|\mathbf{d}_\Delta| = |\mathbf{d}_D| = 0.05 \text{ eV}^{-1}$ in (a) and $|\mathbf{d}_D| = 0.5 \text{ eV}^{-1}$ and $|\mathbf{d}_\Delta| = 0.08 \text{ eV}^{-1}$. All other parameters are the same as in Fig. 3. The insets show shaded regions for which $\int_{-\infty}^{\infty} d\omega I_{p,\times}(\omega) \approx \int_R d\omega I_{p,0}(\omega)$ where R is the domain of the shaded regions, which can be used in Eq. (57) to estimate κ from a measured spectrum.

where the environment is assumed to be in a thermal Gibbs state $\rho_E = \exp(-\beta H_E)/\mathcal{Z}_E$. This assumption is valid in weakly coupled systems where the system and the environment are only weakly correlated even after thermalisation. However, for strongly coupled systems, this assumption is invalidated, and the total Gibbs state $\rho_\beta = \exp(-\beta H)/\mathcal{Z}$ should be used as the initial state where H now refers to the total Hamiltonian. Due to the interaction term, this will no longer be a separable state, and so is rather difficult to model.

An often underappreciated benefit of the polaron transformation is that the separable initial state $\rho_S(0) \otimes \rho_E$ in the polaron frame, models an initial state in the lab frame that is more similar to ρ_β . In our calculations, $\rho_S(0) = |g\rangle\langle g|$, and so $\rho_S(0) \otimes \rho_E$ in the polaron frame becomes $\rho_l(0) = |g\rangle\langle g| \otimes B([D+\Delta]/\nu)\rho_E B(-[D+\Delta]/\nu)$ in the lab frame, which is equal to ρ_β in the limit of negligible transition dipoles and projected onto the ground state. This is the state of the system after decaying to the ground state from a thermalised state, and so

is a good initial state in which to model excitation.

Therefore, to compare the PFME to TEMPO (which operates in the lab frame), we must use the Hamiltonian in Eq. (4) with the initial state $\rho_l(0)$. However, most numerical techniques, including TEMPO, assume that the initial state is $\rho_S(0) \otimes \rho_E$. In Appendix H, we show that this discrepancy can be overcome by deriving an effective Hamiltonian to use in TEMPO such that the environment appears to be in the correct state. For $\rho_S(0) = |g\rangle\langle g|$ in the polaron frame, the required Hamiltonian is $\bar{H} = \bar{H}_0 + \bar{H}_I$, where

$$\bar{H}_0 = \bar{\epsilon}\sigma_z + \bar{V}\sigma_+ + \bar{V}^*\sigma_- + \sum_k \nu_k a_k^\dagger a_k, \quad (60a)$$

$$\bar{H}_I = A_{\Delta\Delta}(\mathcal{I} + \sigma^z) + A_{\mu\bar{\mu}}\sigma_+ + A_{\bar{\mu}\mu}\sigma_-, \quad (60b)$$

and A_{pq} is given in Eq. (5), $\bar{\epsilon} = \epsilon + \chi_{\Delta\Delta}$, $\bar{V} = \chi_{\mu\bar{\mu}}$, where $\chi_{pq} = \sum_k (p_k h_k^* + q_k^* h_k)$ and $h_k = (\Delta_k - D_k)/\nu_k$. We note that because the displacement direction of the polaron transformation is state dependent, the necessary effective Hamiltonian depends on $\rho_S(0)$.

By comparing the Hamiltonians in Eqs. (60) and Eq. (4), we see stark differences if both are assumed to have the initial state $\rho_S(0) \otimes \rho_E$. This includes a renormalisation of the transition energy $\epsilon \rightarrow \bar{\epsilon}$ and the introduction of a driving term \bar{V} . We can understand these differences by noting that the environment is far from equilibrium for a strongly coupled system, and initially, no optical polarons exist in our system. Dynamically created optical polarons effectively introduce a strong restoring force in the system that scales with the strength of the permanent dipoles. The ensuing dynamics are thus considerably different, exacerbating the need for careful consideration of the initial conditions of the physical models we deploy.

B. Angular dependence

An interesting degree of freedom which cannot be explored using numerical techniques is related to the relative angles of the dipole moments, captured within the Ω_{pq} parameters in Eq. (18). Of particular importance is the angle $\theta_{\mu\Delta}$, where $\Omega_{\mu\Delta} = (8\pi/3)|\mathbf{d}_\mu||\mathbf{d}_\Delta|\cos\theta_{\mu\Delta}$, which controls many of the unique effects of strong permanent dipoles given in Eq. (36). For example, when $\Omega_{\mu\Delta} = 0$, the mixed dipole processes described by $\tilde{A}_{nm}^{(\cdot,\cdot)}(s)$ for all n, m except $n = m = 0$ [the $\Gamma_M(\omega)$ terms in Eq. (47) and Fig. 3] vanish, leaving just the sideband-only mixed dipole processes [$\Gamma_{M,SB}(\omega)$ in Eq. (48)] and the transition dipole processes [$\Gamma_T(\omega)$ in Eq. (39)].

If one also assumes that $D_k = 0$, then $\Gamma_{M,SB}(\omega)$ vanishes as well, and the master equation becomes equivalent to that of a Hamiltonian with two independent bosonic baths, one with σ^+ and σ^- interactions and the other with a σ^z interaction, of equal temperature and with the same spectral density. This means that a molecule with $\mathbf{d}_{ee} = -\mathbf{d}_{gg}$ and $\mathbf{d}_\mu \cdot \mathbf{d}_\Delta = 0$ has the same physics as a

molecule without permanent dipoles that interacts with a phonon and photon environment. This also identifies which of the novel processes introduced by permanent dipoles arise due to the non-commutativity of the photon operators on the σ^\pm and σ^z interactions.

In Fig. 6 we plot the decay rate of the PFME as a function of the angle $\theta_{\mu\Delta}$ with $D_k = 0$. The horizontal line is the (vibrational) polaron frame Redfield decay rate generated from the commuting baths model,

$$\begin{aligned} \tilde{H} = & \epsilon\sigma^z + \sum_k \nu_k a_k^\dagger a_k + \sum_q \omega_q b_q^\dagger b_q + A_{\mu\bar{\mu}}\sigma_+ + A_{\bar{\mu}\mu}\sigma_- \\ & + \sigma_z \sum_q (\Delta_q b_q^\dagger + \Delta_q^* b_q), \end{aligned} \quad (61)$$

where A_{pq} is given in Eq. (5) and $[b_q, a_k^\dagger] = 0$. One can see in Fig. 6 that the PFME decay rate varies sinusoidally with $\theta_{\mu\Delta}$. This is due to the dependence of the mixed dipole processes $\Gamma_M(\omega)$ in Eq. (47) on $\Omega_{\mu\Delta}$. The rates are maximal when \mathbf{d}_μ and \mathbf{d}_Δ are orthogonal at which point the rates calculated from H_p and \tilde{H} are the same. For non-zero values of $|\mathbf{d}_\Delta|$ (not shown here), the positions and the number of the maxima and minima can change such that the rates can be made larger than those of the commuting baths model.

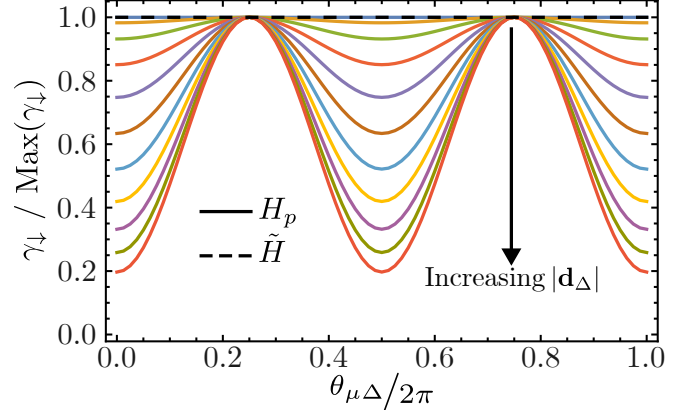


FIG. 6. The normalised decay rate as a function of $\theta_{\mu\Delta}$ and $|\mathbf{d}_\Delta|$. The solid curves are the decay rates calculated from the polaron frame Hamiltonian in Eq. (13), and the dashed line is the decay rate from the Hamiltonian with two commuting baths in Eq. (61). The solid curves have $|\mathbf{d}_\Delta| = [0, 1] \text{ eV}^{-1}$ in intervals of 0.1 and increasing along the direction of the arrow. The rates for parallel and anti-parallel \mathbf{d}_Δ with the same magnitude are identical. The remaining parameters are the same as in Fig. 3.

VII. CONCLUSION

We have studied a quantum optical system with strong permanent dipole moments associated with molecular orbital asymmetry. The optical polaron transformation, which captures the displacement of photonic modes

caused by the permanent dipoles, allows the construction of an optical master equation perturbative only in the transition dipole moment and provides an intuitive formalism to understand the effects associated with the presence of the permanent dipoles on the system dynamics and emission spectrum

We have shown three key results. (1) In Sec. III, we showed that transition and decoherence rates can be engineered for practical application by exploiting permanent dipoles, for example, minimising decoherence, using the novel physical processes explicit in the polaron rate equations we derive. The novel physical processes arising from the permanent dipole are: exciton pumping scaling as $\Omega_{\mu D}$, multiple-photon processes scaling as $\Omega_{\mu D}^2$, $\Omega_{\mu \Delta}^2$ and $\Omega_{\mu D} \Omega_{\mu \Delta}$, a photon sideband with a relative contribution to the emission spectrum scaling as κ^2 , and significant changes to one-photon processes owing to the photon sideband. (2) In Sec. IV, we proved that the optical polaron description provides a much more accurate master equation by comparing it to perturbative master equations and TEMPO. (3) In Sec. V, we indicated four unique and distinguishable features of permanent dipoles in emission spectra, and described possible measurements to obtain $\rho_{ee}(\infty)$, κ and by extension the renormalised energy splitting ϵ' , the driving strength $|V|$, the permanent dipole magnitude $|\mathbf{d}_\Delta|$, and a lower bound for one of $|\mathbf{d}_D|$ or $|\mathbf{d}_\mu|$. The distinguishable features are a photonic sideband, zero photon line centered at $2\bar{\eta}$ due to the exciton driving, altered widths of peaks, and the emergence of a zero frequency peak or Mollow triplet.

There are many interesting features of optical polarons that warrant future exploration. For example,

how the transition rates are affected by embedding the dipole in a structured [71], or anisotropic [72], dielectric medium, common to many biological systems. Moreover, many asymmetric systems couple strongly to vibrational baths and the interplay between photonic and vibrational physics leads to non-additive and non-equilibrium phenomena such as population inversion [51, 73]. How permanent dipoles affect these phenomena is still an open question. Additionally, it has been shown in Refs. [28, 30, 31] that the interplay between the pure dephasing and dissipative interactions leads to non-zero coherences in the steady state. It would be of great interest to explore the nature of the steady state coherences in the optical polaron formalism.

ACKNOWLEDGEMENTS

We would like to thank the Tempo Collaboration for use of the open-source code Oqupy [60]. In particular, we thank Gerald Fux for extremely insightful conversations on the use of Oqupy. D.M.R. also thanks Ahsan Nazir and Owen Diba for helpful discussions.

The work by A.B. was supported by the Leverhulme Quantum Biology Doctoral Training Centre at the University of Surrey funded by a Leverhulme Trust training centre grant number DS-2017-079, and the EPSRC (United Kingdom) Strategic Equipment Grant No. EP/L02263X/1 (EP/M008576/1) and EPSRC (United Kingdom) Grant EP/M027791/1 awards to M.F. D.M.R. is supported by EPSRC (United Kingdom) Grant EP/T517896/1.

[1] H.-P. Breuer, F. Petruccione, *et al.*, *The Theory of Open Quantum Systems* (Oxford University Press on Demand, 2002).

[2] Z. Ficek and S. Swain, *Quantum Interference and Coherence: Theory and Experiments*, Vol. 100 (Springer Science & Business Media, 2005).

[3] A. J. Leggett, S. Chakravarty, A. T. Dorsey, M. P. Fisher, A. Garg, and W. Zwerger, *Dynamics of the Dissipative Two-State System*, *Reviews of Modern Physics* **59**, 1 (1987).

[4] G. S. Agarwal, *Quantum Statistical Theories of Spontaneous Emission and Their Relation to Other Approaches*, *Quantum Optics* , 1 (1974).

[5] P.-H. Chung, C. Tregidgo, and K. Suhling, *Determining a Fluorophore's Transition Dipole Moment from Fluorescence Lifetime Measurements in Solvents of Varying Refractive Index*, *Methods and Applications in Fluorescence* **4**, 045001 (2016).

[6] C. Filippi, F. Buda, L. Guidoni, and A. Sinicropi, *Bathochromic Shift in Green Fluorescent Protein: A Puzzle for QM/MM Approaches*, *Journal of Chemical Theory and Computation* **8**, 112 (2012).

[7] V. Kovarski and O. Prepelitsa, *Effect of a Polar Environment on the Resonant Generation of Higher Optical Harmonics by Dipole Molecules*, *Optics and Spectroscopy* **90**, 351 (2001).

[8] J. Deiglmayr, A. Grochola, M. Repp, O. Dulieu, R. Wester, and M. Weidemüller, *Permanent Dipole Moment of LiCs in the Ground State*, *Physical Review A* **82**, 032503 (2010).

[9] R. Guérout, M. Aymar, and O. Dulieu, *Ground State of the Polar Alkali-Metal-Atom-Strontium Molecules: Potential Energy Curve and Permanent Dipole Moment*, *Physical Review A* **82**, 042508 (2010).

[10] C.-Y. Lin and S. G. Boxer, *Mechanism of Color and Photoacidity Tuning for the Protonated Green Fluorescent Protein Chromophore*, *Journal of the American Chemical Society* **142**, 11032 (2020).

[11] B. Jagatap and W. J. Meath, *Contributions of Permanent Dipole Moments to Molecular Multiphoton Excitation Cross Sections*, *JOSA B* **19**, 2673 (2002).

[12] J. Gilmore and R. H. McKenzie, *Spin Boson Models for Quantum Decoherence of Electronic Excitations of Biomolecules and Quantum Dots in a Solvent*, *Journal of Physics: Condensed Matter* **17**, 1735 (2005).

[13] L. Garziano, V. Macrì, R. Stassi, O. Di Stefano, F. Nori, and S. Savasta, *One Photon can Simultaneously Excite Two or More Atoms*, *Physical Review Letters* **117**,

043601 (2016).

[14] I. Y. Chestnov, V. Shahnazaryan, I. A. Shelykh, and A. P. Alodjants, *Ensemble of Asymmetric Quantum Dots in a Cavity as a Terahertz Laser Source*, *JETP letters* **104**, 169 (2016).

[15] M. Shim and P. Guyot-Sionnest, *Permanent Dipole Moment and Charges in Colloidal Semiconductor Quantum Dots*, *The Journal of Chemical Physics* **111**, 6955 (1999).

[16] M. Antón, F. Carreño, O. Calderón, S. Melle, and E. Cabrera, *Radiation Emission from an Asymmetric Quantum Dot Coupled to a Plasmonic Nanostructure*, *Journal of Optics* **18**, 025001 (2016).

[17] P. Fry, I. Itskevich, D. Mowbray, M. Skolnick, J. Barker, E. O'Reilly, L. Wilson, P. Maksym, M. Hopkinson, M. Al-Khafaji, *et al.*, *Photocurrent Spectroscopy of InAs/GaAs Self-Assembled Quantum Dots: Observation of a Permanent Dipole Moment*, *Physica E: Low-dimensional Systems and Nanostructures* **7**, 408 (2000).

[18] I. Y. Chestnov, V. A. Shahnazaryan, A. P. Alodjants, and I. A. Shelykh, *Terahertz Lasing in Ensemble of Asymmetric Quantum Dots*, *ACS Photonics* **4**, 2726 (2017).

[19] P. Fry, I. Itskevich, D. Mowbray, M. Skolnick, J. Finley, J. Barker, E. O'Reilly, L. Wilson, I. Larkin, P. Maksym, *et al.*, *Inverted Electron-Hole Alignment in InAs-GaAs Self-Assembled Quantum Dots*, *Physical Review Letters* **84**, 733 (2000).

[20] M. Antón, S. Maede-Razavi, F. Carreño, I. Thanopoulos, and E. Paspalakis, *Optical and Microwave Control of Resonance Fluorescence and Squeezing Spectra in a Polar Molecule*, *Physical Review A* **96**, 063812 (2017).

[21] A. Patane, A. Levin, A. Polimeni, F. Schindler, P. Main, L. Eaves, and M. Henini, *Piezoelectric Effects in In 0.5 Ga 0.5 As Self-Assembled Quantum Dots Grown on (311) B GaAs Substrates*, *Applied Physics Letters* **77**, 2979 (2000).

[22] R. J. Warburton, C. Schulhauser, D. Haft, C. Schäflein, K. Karrai, J. M. Garcia, W. Schoenfeld, and P. M. Petroff, *Giant Permanent Dipole Moments of Excitons in Semiconductor Nanostructures*, *Physical Review B* **65**, 113303 (2002).

[23] I. A. Ostapenko, G. Höning, C. Kindel, S. Rodt, A. Strittmatter, A. Hoffmann, and D. Bimberg, *Large Internal Dipole Moment in InGaN/GaN Quantum Dots*, *Applied Physics Letters* **97**, 063103 (2010).

[24] L.-s. Li and A. P. Alivisatos, *Origin and Scaling of the Permanent Dipole Moment in CdSe Nanorods*, *Physical Review Letters* **90**, 097402 (2003).

[25] S. Gupta, Q. Zhang, T. Emrick, and T. P. Russell, “*Self-Corraling*” Nanorods Under an Applied Electric Field, *Nano Letters* **6**, 2066 (2006).

[26] M. MohammadiMasoudi, Z. Hens, and K. Neyts, *Full Alignment of Dispersed Colloidal Nanorods by Alternating Electric Fields*, *RSC Advances* **6**, 55736 (2016).

[27] F. Yoshihara, T. Fuse, S. Ashhab, K. Kakuyanagi, S. Saito, and K. Semba, *Superconducting Qubit-Oscillator Circuit Beyond the Ultrastrong-Coupling Regime*, *Nature Physics* **13**, 44 (2017).

[28] G. Guarnieri, M. Kolář, and R. Filip, *Steady-State Coherences by Composite System-Bath Interactions*, *Physical Review Letters* **121**, 070401 (2018).

[29] Y. S. Greenberg, *Low-Frequency Rabi Spectroscopy of Dissipative Two-Level Systems: Dressed-State Approach*, *Physical Review B* **76**, 104520 (2007).

[30] R. Román-Ancheyta, M. Kolář, G. Guarnieri, and R. Filip, *Enhanced Steady-State Coherence Via Repeated System-Bath Interactions*, *Physical Review A* **104**, 062209 (2021).

[31] A. Purkayastha, G. Guarnieri, M. T. Mitchison, R. Filip, and J. Goold, *Tunable Phonon-Induced Steady-State Coherence in a Double-Quantum-Dot Charge Qubit*, *NPJ Quantum Information* **6**, 1 (2020).

[32] M. Macovei, M. Mishra, and C. H. Keitel, *Population Inversion in Two-Level Systems Possessing Permanent Dipoles*, *Physical Review A* **92**, 013846 (2015).

[33] A. Mírzac, S. Carlig, and M. A. Macovei, *Microwave Multiphoton Conversion Via Coherently Driven Permanent Dipole Systems*, *Physical Review A* **103**, 043719 (2021).

[34] M. Antón, I. Gonzalo, and F. Carreño, *Bichromatically-Controlled Entanglement Between Asymmetric Quantum Dots in a Photonic Cavity*, *Journal of Physics B: Atomic, Molecular and Optical Physics* **54**, 015504 (2020).

[35] F. Oster, C. H. Keitel, and M. Macovei, *Generation of Correlated Photon Pairs in Different Frequency Ranges*, *Physical Review A* **85**, 063814 (2012).

[36] G. Juzeliūnas, L. C. D. Romero, and D. L. Andrews, *Eliminating Ground-State Dipole Moments in Quantum Optics Via Canonical Transformation*, *Physical Review A* **68**, 043811 (2003).

[37] E. Paspalakis, J. Bovatiatsis, and S. Baskoutas, *Effects of Probe Field Intensity in Nonlinear Optical Processes in Asymmetric Semiconductor Quantum Dots*, *Journal of Applied Physics* **114**, 153107 (2013).

[38] J.-Y. Zhao, L.-G. Qin, X.-M. Cai, Q. Lin, and Z.-Y. Wang, *The Effect of a Permanent Dipole Moment on the Polar Molecule Cavity Quantum Electrodynamics*, *Chinese Physics B* **25**, 044202 (2016).

[39] T. Hattori and T. Kobayashi, *Bloch-Siegert Shift in Giant-Dipole Molecules*, *Physical Review A* **35**, 2733 (1987).

[40] G. Scala, K. Slowik, P. Facchi, S. Pascazio, and F. V. Pepe, *Beyond the Rabi Model: Light Interactions with Polar Atomic Systems in a Cavity*, *Physical Review A* **104**, 013722 (2021).

[41] D. M. Rouse, E. Gauger, and B. W. Lovett, *Optimal Power Generation Using Dark States in Dimers Strongly Coupled to Their Environment*, *New Journal of Physics* **21**, 063025 (2019).

[42] S. Tomasi, D. M. Rouse, E. M. Gauger, B. W. Lovett, and I. Kassal, *Environmentally Improved Coherent Light Harvesting*, *The Journal of Physical Chemistry Letters* **12**, 6143 (2021).

[43] F. A. Pollock, D. P. McCutcheon, B. W. Lovett, E. M. Gauger, and A. Nazir, *A Multi-Site Variational Master Equation Approach to Dissipative Energy Transfer*, *New Journal of Physics* **15**, 075018 (2013).

[44] M. Qin, H. Shen, X. Zhao, and X. Yi, *Effects of System-Bath Coupling on a Photosynthetic Heat Engine: A Polaron Master-Equation Approach*, *Physical Review A* **96**, 012125 (2017).

[45] A. Kolli, A. Nazir, and A. Olaya-Castro, *Electronic Excitation Dynamics in Multichromophoric Systems Described Via a Polaron-Representation Master Equation*, *The Journal of Chemical Physics* **135**, 154112 (2011).

[46] D. P. McCutcheon and A. Nazir, *Consistent Treatment of Coherent and Incoherent Energy Transfer Dynamics Using a Variational Master Equation*, *The Journal of Chem-*

ical Physics **135**, 114501 (2011).

[47] A. Nazir and D. P. McCutcheon, *Modelling Exciton-Phonon Interactions in Optically Driven Quantum Dots*, Journal of Physics: Condensed Matter **28**, 103002 (2016).

[48] N. Werren, E. Gauger, and W. Brown, *Light-Harvesting Enhanced by Quantum Ratchet States*, arXiv preprint, arXiv:2209.09978 (2022).

[49] D. M. Rouse, E. M. Gauger, and B. W. Lovett, *Analytic Expression for the Optical Exciton Transition Rates in the Polaron Frame*, Physical Review B **105**, 014302 (2022).

[50] M. Bundgaard-Nielsen, J. Mørk, and E. V. Denning, *Non-Markovian Perturbation Theories for Phonon Effects in Strong-Coupling Cavity Quantum Electrodynamics*, Physical Review B **103**, 235309 (2021).

[51] D. Gribben, D. M. Rouse, J. Iles-Smith, A. Strathearn, H. Maguire, P. Kirton, A. Nazir, E. M. Gauger, and B. W. Lovett, *Exact Dynamics of Nonadditive Environments in Non-Markovian Open Quantum Systems*, PRX Quantum **3**, 010321 (2022).

[52] A. Strathearn, B. W. Lovett, and P. Kirton, *Efficient Real-Time Path Integrals for Non-Markovian Spin-Boson Models*, New Journal of Physics **19**, 093009 (2017).

[53] A. Strathearn, P. Kirton, D. Kilda, J. Keeling, and B. W. Lovett, *Efficient Non-Markovian Quantum Dynamics Using Time-Evolving Matrix Product Operators*, Nature Communications **9**, 3322 (2018).

[54] F. A. Pollock, C. Rodríguez-Rosario, T. Frauenheim, M. Paternostro, and K. Modi, *Non-Markovian Quantum Processes: Complete Framework and Efficient Characterization*, Physical Review A **97**, 012127 (2018).

[55] M. R. Jørgensen and F. A. Pollock, *Exploiting the Causal Tensor Network Structure of Quantum Processes to Efficiently Simulate Non-Markovian Path Integrals*, Physical Review Letters **123**, 240602 (2019).

[56] G. E. Fux, E. P. Butler, P. R. Eastham, B. W. Lovett, and J. Keeling, *Efficient Exploration of Hamiltonian Parameter Space for Optimal Control of Non-Markovian Open Quantum Systems*, Physical Review Letters **126**, 200401 (2021).

[57] D. Gribben, A. Strathearn, G. E. Fux, P. Kirton, and B. W. Lovett, *Using the Environment to Understand Non-Markovian Open Quantum Systems*, Quantum **6**, 847 (2022).

[58] G. E. Fux, D. Kilda, B. W. Lovett, and J. Keeling, *Thermalization of a Spin Chain Strongly Coupled to its Environment*, arXiv preprint, arXiv:2201.05529 (2022).

[59] P. Fowler-Wright, B. W. Lovett, and J. Keeling, *Efficient Many-Body Non-Markovian Dynamics of Organic Polaritons*, Physical Review Letters **129**, 173001 (2022).

[60] The TEMPO collaboration, *OQuPy: A Python 3 Package to Efficiently Compute Non-Markovian Open Quantum Systems*, <http://dx.doi.org/10.5281/zenodo.4428316>. (2020).

[61] M. Babiker and R. Loudon, *Derivation of the Power-Zienau-Woolley Hamiltonian in Quantum Electrodynamics by Gauge Transformation*, Proceedings of the Royal Society of London. A. Mathematical and Physical Sciences **385**, 439 (1983).

[62] A. Stokes and A. Nazir, *A Master Equation for Strongly Interacting Dipoles*, New Journal of Physics **20**, 043022 (2018).

[63] G. D. Mahan, *Many-Particle Physics* (Springer Science & Business Media, 2013).

[64] P. Gaspard and M. Nagaoka, *Slippage of Initial Conditions for the Redfield Master Equation*, The Journal of Chemical Physics **111**, 5668 (1999).

[65] K. Roy-Choudhury and S. Hughes, *Quantum Theory of the Emission Spectrum from Quantum Dots Coupled to Structured Photonic Reservoirs and Acoustic Phonons*, Physical Review B **92**, 205406 (2015).

[66] J. Iles-Smith, D. P. McCutcheon, A. Nazir, and J. Mørk, *Phonon Limit to Simultaneous Near-Unity Efficiency and Indistinguishability in Semiconductor Single Photon Sources*, in *CLEO: QELS_Fundamental Science* (Optical Society of America, 2017) pp. FTu3E-3.

[67] S. Hughes and P. Yao, *Theory of Quantum Light Emission from a Strongly-Coupled Single Quantum Dot Photonic-Crystal Cavity system*, Optics Express **17**, 3322 (2009).

[68] D. F. Walls and G. J. Milburn, *Quantum Optics* (Springer, Berlin, 1994).

[69] D. P. McCutcheon, *Optical Signatures of Non-Markovian Behavior in Open Quantum Systems*, Physical Review A **93**, 022119 (2016).

[70] J.-B. Trebbia, Q. Deplano, P. Tamarat, and B. Lounis, *Tailoring the Superradiant and Subradiant Nature of Two Coherently Coupled Quantum Emitters*, Nature Communications **13**, 1 (2022).

[71] A. Burgess and M. Florescu, *Dynamical Decoherence and Memory Effects in Green Fluorescent Proteins by Dielectric Relaxation*, arXiv preprint, arXiv:2211.09408 (2022).

[72] A. Messinger, N. Westerberg, and S. M. Barnett, *Spontaneous Emission in Anisotropic Dielectrics*, Physical Review A **102**, 013721 (2020).

[73] H. Maguire, J. Iles-Smith, and A. Nazir, *Environmental Nonadditivity and Franck-Condon Physics in Nonequilibrium Quantum Systems*, Physical Review Letters **123**, 093601 (2019).

Appendix A: Displacement operators

Within the appendices, we will regularly use many identities involving displacement operators which are proven in Ref. [47]. This first appendix is dedicated to listing the necessary displacement operator identities. For the purposes of this appendix, we use displacement operators with a single photon mode

$$B(\alpha) = \exp[\alpha a^\dagger - \alpha^* a], \quad (\text{A1})$$

and note that $B(\alpha)^\dagger = B(-\alpha)$ and $B(-\alpha)B(\alpha) = \mathcal{I}$. The first identity is the action of a displacement operator on harmonic operators,

$$B(\pm\alpha)a^\dagger B(\mp\alpha) = a^\dagger \mp \alpha^*, \quad (\text{A2a})$$

$$B(\pm\alpha)aB(\mp\alpha) = a \mp \alpha. \quad (\text{A2b})$$

The second is that the product of two displacement operators is

$$B(\alpha_1)B(\alpha_2) = B(\alpha_1 + \alpha_2)e^{\frac{1}{2}(\alpha_1\alpha_2^* - \alpha_1^*\alpha_2)}. \quad (\text{A3})$$

The third is the action of a displacement operator on the vacuum state to generate a coherent state,

$$B(\alpha)|0\rangle = |\alpha\rangle. \quad (\text{A4})$$

Fourth, that the expectation value of an operator with respect to the thermal state $\rho_E = \exp[-\beta\nu a^\dagger a]/Z_E$ can be written as an integral over coherent states as

$$\text{Tr}_E[O\rho_E] = \frac{1}{\pi N(\nu)} \int_{-\infty}^{\infty} d^2\alpha e^{-\frac{|\alpha|^2}{N(\nu)}} \langle \alpha | O | \alpha \rangle, \quad (\text{A5})$$

where $\int_{-\infty}^{\infty} d^2\alpha = \int_{-\infty}^{\infty} d\Im[\alpha] \int_{-\infty}^{\infty} d\Re[\alpha]$ and $N(\nu) = (e^{\beta\nu} - 1)^{-1}$ is the Bose-Einstein distribution. The final identity is the expectation value of a displacement operator with respect to the vacuum state,

$$\langle 0 | B(\alpha) | 0 \rangle = e^{-\frac{1}{2}|\alpha|^2}. \quad (\text{A6})$$

Appendix B: Calculation of $\langle C \rangle$

Recall from Eq. (14) that

$$C = B(2\delta) \sum_k \left[\mu_k \left(a_k^\dagger + \frac{\Delta_k^* - D_k^*}{\nu_k} \right) + \bar{\mu}_k^* \left(a_k + \frac{\Delta_k - D_k}{\nu_k} \right) \right], \quad (\text{B1})$$

where we have defined $\delta_k = \Delta_k/\nu_k$. In order to calculate $\langle C \rangle = \text{Tr}_E[C\rho_E]$ we require $\langle B(2\delta) \rangle$, $\langle B(2\delta)a_k^\dagger \rangle$ and $\langle B(2\delta)a_k \rangle$. We will perform these calculations explicitly, because the polaron frame environment correlation functions require analogous, but more algebraically involved, mathematics. We do the calculations with a single photonic mode, where $B(\alpha) = \exp[\alpha a^\dagger - \alpha a]$, and reinstate the multimode summations at the end. To calculate the expectation values we aim to use Eq. (A5).

Starting with $\langle B(2\delta) \rangle$, we first evaluate the integrand of Eq. (A5) as

$$\begin{aligned} \langle \alpha | B(2\delta) | \alpha \rangle &= \langle 0 | B(-\alpha) B(2\delta) B(\alpha) | 0 \rangle \\ &= \langle 0 | B(2\delta) | 0 \rangle e^{2\delta\alpha^* - 2\delta^*\alpha} \\ &= e^{-2|\delta|^2} e^{2\delta\alpha^* - 2\delta^*\alpha}, \end{aligned} \quad (\text{B2})$$

where in the first equality we have used Eq. (A4) twice, in the second equality Eq. (A3) twice and in the final equality Eq. (A6). Substituting Eq. (B2) into Eq. (A4) then yields

$$\langle B(2\delta) \rangle = e^{-2|\delta|^2 \coth(\frac{\beta\nu}{2})} \equiv \kappa. \quad (\text{B3})$$

Evaluating $\langle B(2\delta)a^\dagger \rangle$ follows a similar procedure. However one must now use Eqs. (A2) to move the creation operator such that it annihilates with the vacuum bra-state $\langle 0 |$. That is,

$$\begin{aligned} \langle \alpha | B(2\delta)a^\dagger | \alpha \rangle &= \langle 0 | B(-\alpha) B(2\delta)a^\dagger | \alpha \rangle \\ &= \langle 0 | B(-\alpha) [a^\dagger - 2\delta^*] B(2\delta) | \alpha \rangle \\ &= [\alpha^* - 2\delta^*] \langle \alpha | B(2\delta) | \alpha \rangle \\ &= [\alpha^* - 2\delta^*] e^{-2|\delta|^2} e^{2\delta\alpha^* - 2\delta^*\alpha}. \end{aligned} \quad (\text{B4})$$

Substituting Eq. (B4) into Eq. (A5) and performing the integrations yields

$$\langle B(2\delta)a^\dagger \rangle = -2\kappa\delta^* [1 + N(\nu)]. \quad (\text{B5})$$

The final expectation value, $\langle B(2\delta)a \rangle$, is easier to calculate because a annihilates with $|0\rangle$. One finds that

$$\langle \alpha | B(2\delta)a | \alpha \rangle = \alpha e^{-2|\delta|^2} e^{2\delta\alpha^* - 2\delta^*\alpha}, \quad (\text{B6})$$

and so

$$\langle B(2\delta)a \rangle = 2\kappa\delta N(\nu). \quad (\text{B7})$$

Collecting the expectation values in Eqs. (B3), (B5) and (B7) and substituting these into $\langle C \rangle$ with C given in Eq. (B1) yields

$$\langle C \rangle = \kappa \left[\coth\left(\frac{\beta\nu}{2}\right) \frac{\bar{\mu}^*\Delta - \mu\Delta^*}{\nu} - \frac{\mu D^* + \bar{\mu}^* D}{\nu} \right]. \quad (\text{B8})$$

Since $\mathbf{d}_\Delta \in \mathfrak{R}$, we find that $\bar{\mu}^*\Delta - \mu\Delta^* = 0$. Therefore,

$$\langle C \rangle = -\kappa \frac{\mu D^* + \bar{\mu}^* D}{\nu}. \quad (\text{B9})$$

Reinstating the summation of modes and taking the continuum limit, one arrives at Eq. (21) after noting that $\mu_k D_k^* + \bar{\mu}_k^* D_k = 2(\mathbf{d}_\mu \cdot \mathbf{e}_k)(\mathbf{d}_D \cdot \mathbf{e}_k)|f_k|^2$ and using Eq. (17).

Appendix C: Non-secular master equations

1. The PFME and DFME

The non-secular master equation in both the polaron and displaced frames have the same forms, only differing in which operators enter the two-time correlation functions, and therefore the rates and energies in the master equation below will be different in either. We find that

$$\partial_t \rho_{++}(t) = -\gamma_{\downarrow} \rho_{++}(t) + \gamma_{\uparrow} \rho_{--}(t) + \bar{\gamma} \rho_{-+}(t) + \bar{\gamma}^* \rho_{+-}(t), \quad (\text{C1a})$$

$$\partial_t \rho_{+-}(t) = -[\gamma_d + 2i\bar{\eta}] \rho_{+-}(t) + k_1 \rho_{-+}(t) + k_- \rho_{--}(t) + k_+^* \rho_{++}(t), \quad (\text{C1b})$$

and $\partial_t \rho_{--}(t) = -\partial_t \rho_{++}(t)$ and $\partial_t \rho_{-+}(t) = \partial_t \rho_{+-}(t)^\dagger$. As defined in the main text, the secular rates are

$$\gamma_{\downarrow} = \gamma_{\mp\mp}(\pm 2\eta), \quad (\text{C2})$$

$$\gamma_d = \frac{1}{2} [\gamma_{\uparrow} + \gamma_{\downarrow}] + 2\gamma_{zz}(0), \quad (\text{C3})$$

$$2\bar{\eta} = 2\eta + \Im[\Gamma_{--}(2\eta) - \Gamma_{++}(-2\eta)]. \quad (\text{C4})$$

The rates are written in terms of the Markovian ECFs as

$$\Gamma_{\alpha\beta}(\omega) = \int_0^\infty ds e^{i\omega s} \langle g_\alpha^\dagger(s) g_\beta(0) \rangle, \quad (\text{C5})$$

for $\alpha \in \{z, +, -\}$, and it is the expressions for g_α that vary between the PMFE and DFME, and these are given in the main text in Eqs. (28) and Appendix E, respectively. The non-secular rates are

$$\bar{\gamma} = \Gamma_{-z}(0) + \Gamma_{+z}(0)^* \quad (\text{C6a})$$

$$k_1 = \Gamma_{-+}(-2\eta) + \Gamma_{+-}(2\eta)^*, \quad (\text{C6b})$$

$$k_{\pm} = \mp\Gamma_{\pm z}(0) \pm \Gamma_{\mp z}(0)^* \pm 2\Gamma_{z\mp}(\pm 2\eta) \quad (\text{C6c})$$

We evaluate $\Gamma_{\alpha\beta}(\omega)$ for the polaron frame in Appendix D and for the displaced frame in Appendix E.

Notice that if the coherences are initially zero ($\rho_{+-}(0) = \rho_{-+}(0) = 0$) then if $k_- = k_+ = 0$ as well, the coherences will be zero at all times t . This occurs in the polaron frame if $|\mathbf{d}_D| \rightarrow 0$ since $g_z \propto \sin(\varphi) \rightarrow 0$, i.e. the eigenstates fully localise, but this does not happen in the displaced frame in the same limit because g_z^d does not become zero.

2. The LFME

The lab frame master equation has the same structure as Eqs. (C1), although there is no eigenbasis, and so the eigenstates localise onto the lab basis $|+\rangle \rightarrow |e\rangle$ and $|-\rangle \rightarrow |g\rangle$. Additionally, because the lab frame interaction Hamiltonian [see Eq. (4)] has an system-identity interaction as well as the σ_z , σ_+ and σ_- interactions that appear in the displaced and polaron frame Hamiltonians, the rates in the LFME have additional terms beyond those in the PFME or DFME given in the previous subsection.

The LFME is

$$\partial_t \rho_{ee}(t) = -\gamma_{\downarrow}^l \rho_{ee}(t) + \gamma_{\uparrow}^l \rho_{gg}(t) + \bar{\gamma}^l \rho_{ge}(t) + \bar{\gamma}^{l*} \rho_{eg}(t), \quad (\text{C7a})$$

$$\partial_t \rho_{eg}(t) = -[\gamma_d^l + 2i\bar{\epsilon}] \rho_{eg}(t) + k_1^l \rho_{ge}(t) + k_-^l \rho_{gg}(t) + k_+^{l*} \rho_{ee}(t), \quad (\text{C7b})$$

and $\partial_t \rho_{gg}(t) = -\partial_t \rho_{ee}(t)$ and $\partial_t \rho_{eg}(t) = \partial_t \rho_{ge}(t)^\dagger$. The secular rates are

$$\gamma_{\downarrow}^l = \gamma_{\bar{\mu}\mu, \bar{\mu}\mu}^l(2\eta), \quad (\text{C8})$$

$$\gamma_{\uparrow}^l = \gamma_{\mu\bar{\mu}, \mu\bar{\mu}}^l(-2\eta), \quad (\text{C9})$$

$$\gamma_d^l = \frac{1}{2} [\gamma_{\uparrow}^l + \gamma_{\downarrow}^l] + 2\gamma_{\Delta\Delta, \Delta\Delta}^l(0), \quad (\text{C10})$$

$$2\bar{\epsilon} = 2\epsilon + S_{\bar{\mu}\mu, \bar{\mu}\mu}^l(2\epsilon) - S_{\mu\bar{\mu}, \mu\bar{\mu}}^l(-2\epsilon) + 4S_{\Delta\Delta, DD}^l(0), \quad (\text{C11})$$

and the non-secular rates are

$$\bar{\gamma}^l = \Gamma_{\bar{\mu}\mu, \Delta\Delta}^l(0) + \Gamma_{\mu\bar{\mu}, \Delta\Delta}^l(0)^* + \tilde{k}^l, \quad (\text{C12})$$

$$k_1^l = \Gamma_{\bar{\mu}\mu, \mu\bar{\mu}}^l(-2\epsilon) + \Gamma_{\mu\bar{\mu}, \bar{\mu}\mu}^l(2\epsilon)^*, \quad (\text{C13})$$

$$k_+^l = -\Gamma_{\mu\bar{\mu}, \Delta\Delta}^l(0) + \Gamma_{\bar{\mu}\mu, \Delta\Delta}^l(0)^* + 2\Gamma_{\Delta\Delta, \bar{\mu}\mu}^l(2\eta) - \tilde{k}^{l*}, \quad (\text{C14})$$

$$k_-^l = +\Gamma_{\bar{\mu}\mu, \Delta\Delta}^l(0) - \Gamma_{\mu\bar{\mu}, \Delta\Delta}^l(0)^* - 2\Gamma_{\Delta\Delta, \mu\bar{\mu}}^l(-2\eta) + \tilde{k}^l, \quad (\text{C15})$$

where

$$\tilde{k}^l = -i [S_{\bar{\mu}\mu, DD}^l(0) + S_{\mu\bar{\mu}, DD}^l(0)] + \frac{\gamma_{\mu\bar{\mu}, DD}^l(0) - \gamma_{\bar{\mu}\mu, DD}^l(0)}{2}. \quad (\text{C16})$$

These are written in terms of the lab frame ECF by,

$$\Gamma_{pq, rs}^l(\omega) = \int_0^\infty ds e^{i\omega s} \langle A_{pq}^\dagger(s) A_{rs}(0) \rangle \equiv \frac{1}{2} \gamma_{pq, rs}^l(\omega) + i S_{pq, rs}^l(\omega), \quad (\text{C17})$$

where A_{pq} is defined in Eq. (5). Substituting Eq. (5) into the ECF and using that $\langle a_k^\dagger a_{k'} \rangle = \delta_{kk'} N(\nu_{\mathbf{k}})$, $\langle a_k a_{k'}^\dagger \rangle = \delta_{kk'} \tilde{N}(\nu_{\mathbf{k}})$ where $\tilde{N}(\nu) = 1 + N(\nu)$ and that other combinations equal zero, leads to

$$\gamma_{pq, rs}^l(\omega) = 2\pi \left[\Omega_{\bar{p}r} J(\omega) \tilde{N}(\omega) + \Omega_{q\bar{s}} J(-\omega) N(-\omega) \right], \quad (\text{C18a})$$

$$S_{pq, rs}^l(\omega) = \mathcal{P} \int_0^\infty d\nu J(\nu) \left[\Omega_{\bar{p}r} \frac{\tilde{N}(\nu)}{\omega - \nu} + \Omega_{q\bar{s}} \frac{N(\nu)}{\omega + \nu} \right]. \quad (\text{C18b})$$

As usual, an overbar in the subscript denotes the complex conjugate of the dipole vector e.g. $\Omega_{\bar{p}r} = (8\pi/3)(\mathbf{d}_p^* \cdot \mathbf{d}_r)$. Also recall that $J(\omega \leq 0) = 0$ and $\mathbf{d}_\Delta \in \Re$. Note that if $D_k = 0$, the DFME and LFME are identical.

Appendix D: Calculation of the polaron frame two-time correlation functions

The environment correlation functions, which determine the second order Born-Markov rates, depend on the two-time correlation functions $\langle g_\alpha^\dagger(s)g_\beta(0) \rangle$ for $\alpha, \beta \in \{z, +, -\}$ where recalling from Eq. (28),

$$g_z = \frac{1}{2} \sin(\varphi) [\mathcal{C} e^{i\theta} + \mathcal{C}^\dagger e^{-i\theta}], \quad (\text{D1a})$$

$$g_+ = \left[\cos^2\left(\frac{\varphi}{2}\right) \mathcal{C} e^{i\theta} - \sin^2\left(\frac{\varphi}{2}\right) \mathcal{C}^\dagger e^{-i\theta} \right], \quad (\text{D1b})$$

and $g_- = g_+^\dagger$ where $\mathcal{C} = C - \kappa V$ and

$$C = B_+ \sum_k \left[\mu \left(a_k^\dagger + \frac{\Delta_k^* - D_k^*}{\nu_{\mathbf{k}}} \right) + \bar{\mu}_k^* \left(a_k + \frac{\Delta_k - D_k}{\nu_{\mathbf{k}}} \right) \right], \quad (\text{D2})$$

where $B_\pm \equiv B(\pm 2\Delta/\nu)$ which is given in Eq. (14). The interaction picture form of the relevant operators are,

$$a_k(s) = a_k e^{-i\nu_{\mathbf{k}} s}, \quad (\text{D3})$$

$$B_\pm(s) = B \left(\pm \frac{2\Delta}{\nu} e^{i\nu s} \right). \quad (\text{D4})$$

1. Preliminary calculations

All $\langle g_\alpha^\dagger(s)g_\beta(0) \rangle$ depend on four two-time correlation functions: $\langle C^\dagger(s)C(0) \rangle$, $\langle C(s)C^\dagger(0) \rangle$, $\langle C(s)C(0) \rangle$, and $\langle C^\dagger(s)C^\dagger(0) \rangle$. Each of these in turn depends on either six or nine unique two-time correlation functions involving a_k , a_k^\dagger and $B_\pm = B(\pm 2\delta_k)$ where $\delta_k = \Delta_k/\nu_{\mathbf{k}}$. In this Appendix, we list the results of all necessary two-time correlation functions which are each derived using the same mathematics as in the explicit examples in Appendix B.

a. $\langle C^\dagger(s)C(0) \rangle$

To calculate this two-time correlation function, we require:

$$\langle B_-(s)B_+(0) \rangle = \kappa^2 e^\phi, \quad (\text{D5a})$$

$$\langle a_k^\dagger B_-(s)B_+(0) \rangle = -N_{\mathbf{k}} x_k^* \kappa^2 e^\phi, \quad (\text{D5b})$$

$$\langle a_k B_-(s)B_+(0) \rangle = \tilde{N}_{\mathbf{k}} x_k \kappa^2 e^\phi, \quad (\text{D5c})$$

$$\langle B_-(s)B_+(0)a_k^\dagger \rangle = -\tilde{N}_{\mathbf{k}} x_k^* \kappa^2 e^\phi, \quad (\text{D5d})$$

$$\langle B_-(s)B_+(0)a_k \rangle = N_{\mathbf{k}} x_k \kappa^2 e^\phi, \quad (\text{D5e})$$

$$\langle a_k^\dagger B_-(s)B_+(0)a_q^\dagger \rangle = N_{\mathbf{k}} \tilde{N}_{\mathbf{q}} x_k^* x_q^* \kappa^2 e^\phi, \quad (\text{D5f})$$

$$\langle a_k B_-(s)B_+(0)a_q \rangle = \tilde{N}_{\mathbf{k}} N_{\mathbf{q}} x_k x_q \kappa^2 e^\phi, \quad (\text{D5g})$$

$$\langle a_k^\dagger B_-(s)B_+(0)a_q \rangle = (-N_{\mathbf{k}} N_{\mathbf{q}} x_k^* x_q + N_{\mathbf{k}} \delta_{kq}) \kappa^2 e^\phi, \quad (\text{D5h})$$

$$\langle a_k B_-(s)B_+(0)a_q^\dagger \rangle = \left(-\tilde{N}_{\mathbf{k}} \tilde{N}_{\mathbf{q}} x_k x_q^* + \tilde{N}_{\mathbf{k}} \delta_{kq} \right) \kappa^2 e^\phi, \quad (\text{D5i})$$

where, for brevity, $N_{\mathbf{k}} \equiv N(\nu_{\mathbf{k}})$ is the Bose-Einstein distribution, $\tilde{N}_{\mathbf{k}} \equiv \tilde{N}(\nu_{\mathbf{k}}) = 1 + N(\nu_{\mathbf{k}})$, $\phi \equiv \phi(s)$ given in Eq. (19), $\kappa^2 = \exp[-\phi(0)]$, and finally

$$x_k \equiv x_k(s) = 2\delta_k (1 - e^{i\nu_{\mathbf{k}} s}). \quad (\text{D6})$$

Substituting Eqs. (D5) into the two-time correlation function we find that,

$$\langle C^\dagger(s)C(0) \rangle = \kappa^2 e^{\phi(s)} \left[\sum_k \left(|\bar{\mu}_k|^2 N_{\mathbf{k}} e^{i\nu_{\mathbf{k}} s} + |\mu_{\mathbf{k}}|^2 \tilde{N}_{\mathbf{k}} e^{-i\nu_{\mathbf{k}} s} \right) + \sum_{n,m=-1}^1 \sum_{kq} A_{nm}^{(\dagger,\cdot)}(k, q) e^{in\nu_{\mathbf{k}} s} e^{im\nu_{\mathbf{q}} s} \right] \quad (\text{D7})$$

where $A_{nm}^{(\dagger,\cdot)}(k, q)$ are coefficients second order in both the transition dipole moments and permanent dipole moments. The superscript (\dagger, \cdot) indicates that this matrix contains the coefficients for the expectation value of $\langle C^\dagger(s)C(0) \rangle$. We write the coefficients in matrix notation for brevity, using the format

$$A^{(\dagger,\cdot)}(k, q) = \begin{pmatrix} A_{-1,-1}^{(\dagger,\cdot)}(k, q) & A_{-1,0}^{(\dagger,\cdot)}(k, q) & A_{-1,1}^{(\dagger,\cdot)}(k, q) \\ A_{0,-1}^{(\dagger,\cdot)}(k, q) & A_{0,0}^{(\dagger,\cdot)}(k, q) & A_{0,1}^{(\dagger,\cdot)}(k, q) \\ A_{1,-1}^{(\dagger,\cdot)}(k, q) & A_{1,0}^{(\dagger,\cdot)}(k, q) & A_{1,1}^{(\dagger,\cdot)}(k, q) \end{pmatrix}. \quad (\text{D8})$$

Written in this notation, one finds that

$$A^{(\dagger,\cdot)}(k, q) = 4 \frac{|f_{\mathbf{k}}|^2}{\nu_{\mathbf{k}}} \frac{|f_{\mathbf{q}}|^2}{\nu_{\mathbf{q}}} \mu_k^{0*} \mu_q^0 \begin{pmatrix} \tilde{N}_{\mathbf{k}} \Delta_k^0 \tilde{N}_{\mathbf{q}} \Delta_q^0 & -\tilde{N}_{\mathbf{k}} \Delta_k^0 D_q^0 & -\tilde{N}_{\mathbf{k}} \Delta_k^0 N_q \Delta_q^0 \\ -\tilde{N}_{\mathbf{q}} \Delta_q^0 D_k^0 & D_k^0 D_q^0 & D_k^0 N_{\mathbf{q}} \Delta_q^0 \\ -N_{\mathbf{k}} \Delta_k^0 \tilde{N}_{\mathbf{q}} \Delta_q^0 & N_{\mathbf{k}} \Delta_k^0 D_q^0 & N_{\mathbf{k}} \Delta_k^0 N_{\mathbf{q}} \Delta_q^0 \end{pmatrix}, \quad (\text{D9})$$

where we have arbitrarily (and without loss of generality for the single dipole system) chosen the position of the dipole to be $\mathbf{r} = \mathbf{0}$ such that we may write $\mu_k = i\mu_k^0 f_{\mathbf{k}}$, $\bar{\mu}_k = i\mu_k^{0*} f_{\mathbf{k}}$, $\Delta_k = i\Delta_k^0 f_{\mathbf{k}}$ and $D_k = iD_k^0 f_{\mathbf{k}}$ with $\mu_k^0 = \mathbf{d}_{\mu} \cdot \mathbf{e}_k$, $\Delta_k^0 = \mathbf{d}_{\Delta} \cdot \mathbf{e}_k$ and $D_k^0 = \mathbf{d}_D \cdot \mathbf{e}_k$.

If one ignores the factor of $\kappa^2 \exp[\phi(s)]$, the first term in Eq. (D7) will lead to the standard optical master equation rates describing photon emission and absorption scaling with the magnitude squared of the transition dipole strength. The second term in Eq. (D7) describes corrections to the standard optical master equation rates that are second order in both the permanent dipole moments and the transition dipole moments. The factor of $\kappa^2 \exp[\phi(s)]$ accounts for higher order permanent dipole contributions.

Moreover, the second term in Eq. (D7) along with Eq. (D9) reveals the physical processes induced by the permanent dipoles. Since this is a second order term, each term n and m describes two simultaneous processes into the k and q modes, respectively. When n or m equal -1 the processes are photon emission, when n or m equal 0 the processes are non-radiative, and when n or m equal $+1$ the processes are photon absorption. This can be seen by both the frequency dependence of the exponential phase factors in Eq. (D7) and by the dependence of the matrix elements on $\tilde{N}_{\mathbf{k}}$, $N_{\mathbf{k}}$, or neither. Additionally, one can see that radiative terms scale as Δ_k^0 whilst non-radiative terms scale as D_k^0 . For example, the $(n, m) = (1, 0)$ term describes photon absorption into the k mode and a non-radiative process into the q mode, scaling as $A_{1,0}^{(\dagger,\cdot)}(k, q) \propto N_{\mathbf{k}} \Delta_k^0 D_q^0$.

Finally, we take the continuum limit to obtain

$$\langle C^\dagger(s)C(0) \rangle = \kappa^2 e^{\phi(s)} \left[\Omega_{\mu\bar{\mu}} \int_0^\infty d\nu J(\nu) \left(N(\nu) e^{i\nu s} + \tilde{N}(\nu) e^{-i\nu s} \right) + \sum_{n,m=-1}^1 \tilde{A}_{nm}^{(\dagger,\cdot)}(s) \right], \quad (\text{D10})$$

where we have defined the two-dimensional Fourier transform

$$\tilde{A}_{nm}^{(\dagger,\cdot)}(s) = \int_0^\infty d\nu \int_0^\infty d\nu' A_{nm}^{(\dagger,\cdot)}(\nu, \nu') e^{i\nu s} e^{im\nu' s}, \quad (\text{D11})$$

and the continuum limit of the coefficients can be written in the matrix representation as

$$A^{(\dagger,\cdot)}(\nu, \nu') = 4 \frac{J(\nu)}{\nu} \frac{J(\nu')}{\nu'} \times \begin{pmatrix} \Omega_{\bar{\mu}\Delta} \Omega_{\mu\Delta} \tilde{N}(\nu) \tilde{N}(\nu') & -\Omega_{\bar{\mu}\Delta} \Omega_{\mu D} \tilde{N}(\nu) & -\Omega_{\bar{\mu}\Delta} \Omega_{\mu\Delta} \tilde{N}(\nu) N(\nu') \\ -\Omega_{\bar{\mu}D} \Omega_{\mu\Delta} \tilde{N}(\nu') & \Omega_{\bar{\mu}D} \Omega_{\mu D} & \Omega_{\bar{\mu}D} \Omega_{\mu\Delta} N(\nu') \\ -\Omega_{\bar{\mu}\Delta} \Omega_{\mu\Delta} N(\nu) \tilde{N}(\nu') & \Omega_{\bar{\mu}\Delta} \Omega_{\mu D} N(\nu) & \Omega_{\bar{\mu}\Delta} \Omega_{\mu\Delta} N(\nu) N(\nu') \end{pmatrix}. \quad (\text{D12})$$

$$b. \quad \langle C(s)C^\dagger(0) \rangle$$

To calculate this two-time correlation function, we require:

$$\langle B_+(s)B_-(0) \rangle = \kappa^2 e^\phi, \quad (D13a)$$

$$\langle B_+(s)a_k^\dagger B_-(0) \rangle = \left(-2\delta_k^* - \tilde{N}_k y_k^* \right) \kappa^2 e^\phi, \quad (D13b)$$

$$\langle B_+(s)a_k B_-(0) \rangle = (-2\delta_k + N_k y_k) \kappa^2 e^\phi, \quad (D13c)$$

$$\langle B_+(s)a_k^\dagger a_q^\dagger B_-(0) \rangle = \left(-2\delta_k^* - \tilde{N}_k y_k^* \right) \left(-2\delta_q^* - \tilde{N}_q y_q^* \right) \kappa^2 e^\phi, \quad (D13d)$$

$$\langle B_+(s)a_k a_q B_-(0) \rangle = (-2\delta_k + N_k y_k) (-2\delta_q + N_q y_q) \kappa^2 e^\phi, \quad (D13e)$$

$$\langle B_+(s)a_k^\dagger a_q B_-(0) \rangle = \left[N_k \delta_{kq} + \left(-2\delta_k^* - \tilde{N}_k y_k^* \right) (-2\delta_q + N_q y_q) \right] \kappa^2 e^\phi, \quad (D13f)$$

$$\langle B_+(s)a_k a_q^\dagger B_-(0) \rangle = \left[\tilde{N}_k \delta_{kq} + (-2\delta_k + N_k y_k) \left(-2\delta_q^* - \tilde{N}_q y_q^* \right) \right] \kappa^2 e^\phi, \quad (D13g)$$

where

$$y_k \equiv y_k(s) = 2\delta_k (e^{i\nu_k s} - 1). \quad (D14)$$

Substituting Eqs. (D13) into the two-time correlation function and taking the continuum limit one obtains

$$\langle C(s)C^\dagger(0) \rangle = \kappa^2 e^{\phi(s)} \left[\Omega_{\mu\bar{\mu}} \int_0^\infty d\nu J(\nu) \left(N(\nu) e^{i\nu s} + \tilde{N}(\nu) e^{-i\nu s} \right) + \sum_{n,m=-1}^1 \tilde{A}_{nm}^{(\cdot,\dagger)}(s) \right], \quad (D15)$$

which is the same as Eq. (D10) except for the form of the coefficients in the second term. Analogously to Eq. (D11), we have defined

$$\tilde{A}_{nm}^{(\cdot,\dagger)}(s) = \int_0^\infty d\nu \int_0^\infty d\nu' A_{nm}^{(\cdot,\dagger)}(\nu, \nu') e^{in\nu s} e^{im\nu' s}, \quad (D16)$$

where written in the matrix notation,

$$A^{(\cdot,\dagger)}(\nu, \nu') = 4 \frac{J(\nu)}{\nu} \frac{J(\nu')}{\nu'} \times \begin{pmatrix} \Omega_{\mu\Delta} \Omega_{\bar{\mu}\Delta} \tilde{N}(\nu) \tilde{N}(\nu') & \Omega_{\mu\Delta} \Omega_{\bar{\mu}D} \tilde{N}(\nu) & -\Omega_{\mu\Delta} \Omega_{\bar{\mu}\Delta} \tilde{N}(\nu) N(\nu') \\ \Omega_{\mu D} \Omega_{\bar{\mu}\Delta} \tilde{N}(\nu') & \Omega_{\mu D} \Omega_{\bar{\mu}D} & -\Omega_{\mu D} \Omega_{\bar{\mu}\Delta} N(\nu') \\ -\Omega_{\mu\Delta} \Omega_{\bar{\mu}\Delta} N(\nu) \tilde{N}(\nu') & -\Omega_{\mu\Delta} \Omega_{\bar{\mu}D} N(\nu) & \Omega_{\mu\Delta} \Omega_{\bar{\mu}\Delta} N(\nu) N(\nu') \end{pmatrix}. \quad (D17)$$

Note that $\tilde{A}^{(\cdot,\dagger)}(\nu, \nu')$ is the same as $\tilde{A}^{(\dagger,\cdot)}(\nu, \nu')$ up to the placement of the four factors of -1 and the $\bar{\mu}$ position, which we will see to be true for the remaining two-time correlation functions. Thus, the physical interpretation of the correlation functions $\langle C^\dagger(s)C(0) \rangle$ and $\langle C(s)C^\dagger(0) \rangle$ are the same.

$$c. \quad \langle C^\dagger(s)C^\dagger(0) \rangle$$

To calculate this two-time correlation function, we require:

$$\langle B_-(s)B_-(0) \rangle = \kappa^2 e^{-\phi}, \quad (D18a)$$

$$\langle a_k^\dagger B_-(s)B_-(0) \rangle = -N_{\mathbf{k}} z_k^* \kappa^2 e^{-\phi}, \quad (D18b)$$

$$\langle a_k B_-(s)B_-(0) \rangle = \tilde{N}_{\mathbf{k}} z_k \kappa^2 e^{-\phi}, \quad (D18c)$$

$$\langle B_-(s)a_k^\dagger B_-(0) \rangle = \left(-\tilde{N}_{\mathbf{k}} z_k^* - 2\delta_k^* \right) \kappa^2 e^{-\phi}, \quad (D18d)$$

$$\langle B_-(s)a_k B_-(0) \rangle = (N_{\mathbf{k}} z_k - 2\delta_k) \kappa^2 e^{-\phi}, \quad (D18e)$$

$$\langle a_k^\dagger B_-(s)a_q^\dagger B_-(0) \rangle = -N_{\mathbf{k}} z_k^* \left(-\tilde{N}_{\mathbf{q}} z_q^* - 2\delta_q^* \right) \kappa^2 e^{-\phi}, \quad (D18f)$$

$$\langle a_k B_-(s)a_q B_-(0) \rangle = \tilde{N}_{\mathbf{k}} z_k (N_{\mathbf{q}} z_q - 2\delta_q) \kappa^2 e^{-\phi}, \quad (D18g)$$

$$\langle a_k^\dagger B_-(s)a_q B_-(0) \rangle = [N_{\mathbf{k}} \delta_{kq} - N_{\mathbf{k}} z_k (N_{\mathbf{q}} z_q - 2\delta_q)] \kappa^2 e^{-\phi}, \quad (D18h)$$

$$\langle a_k B_-(s)a_q^\dagger B_-(0) \rangle = \left[\tilde{N}_{\mathbf{k}} \delta_{kq} + \tilde{N}_{\mathbf{k}} z_k (N_{\mathbf{q}} z_q - 2\delta_q) \right] \kappa^2 e^{-\phi}, \quad (D18i)$$

where

$$z_k \equiv z_k(s) = -2\delta_k (e^{i\nu_{\mathbf{k}} s} + 1). \quad (D19)$$

Substituting Eqs. (D18) into the two-time correlation function and taking the continuum limit one obtains

$$\langle C^\dagger(s)C^\dagger(0) \rangle = \kappa^2 e^{-\phi(s)} \left[\Omega_{\bar{\mu}\bar{\mu}} \int_0^\infty d\nu J(\nu) \left(N(\nu) e^{i\nu s} + \tilde{N}(\nu) e^{-i\nu s} \right) + \sum_{n,m=-1}^1 \tilde{A}_{nm}^{(\dagger,\dagger)}(s) \right], \quad (D20)$$

Analogously to Eq. (D11), we have defined

$$\tilde{A}_{nm}^{(\dagger,\dagger)}(s) = \int_0^\infty d\nu \int_0^\infty d\nu' A_{nm}^{(\dagger,\dagger)}(\nu, \nu') e^{i\nu s} e^{i\nu' s}, \quad (D21)$$

where written in the matrix notation,

$$A^{(\dagger,\dagger)}(\nu, \nu') = 4 \frac{J(\nu)}{\nu} \frac{J(\nu')}{\nu'} \times \begin{pmatrix} -\Omega_{\bar{\mu}\Delta} \Omega_{\bar{\mu}\Delta} \tilde{N}(\nu) \tilde{N}(\nu') & \Omega_{\bar{\mu}\Delta} \Omega_{\bar{\mu}D} \tilde{N}(\nu) & \Omega_{\bar{\mu}\Delta} \Omega_{\bar{\mu}\Delta} \tilde{N}(\nu) N(\nu') \\ -\Omega_{\bar{\mu}D} \Omega_{\bar{\mu}\Delta} \tilde{N}(\nu') & \Omega_{\bar{\mu}D} \Omega_{\bar{\mu}D} & \Omega_{\bar{\mu}D} \Omega_{\bar{\mu}\Delta} N(\nu') \\ \Omega_{\bar{\mu}\Delta} \Omega_{\bar{\mu}\Delta} N(\nu) \tilde{N}(\nu') & -\Omega_{\bar{\mu}\Delta} \Omega_{\bar{\mu}D} N(\nu) & -\Omega_{\bar{\mu}\Delta} \Omega_{\bar{\mu}\Delta} N(\nu) N(\nu') \end{pmatrix}. \quad (D22)$$

Eq. (D20) is only different from Eq. (D12) due to the position of the four factors of -1 in $A^{(\dagger,\dagger)}(\nu, \nu')$, $\phi(s) \rightarrow -\phi(s)$, and the lack of μ subscripts.

$$d. \quad \langle C(s)C(0) \rangle$$

To calculate this two-time correlation function we require:

$$\langle B_+(s)B_+(0) \rangle = \kappa^2 e^{-\phi}, \quad (\text{D23a})$$

$$\langle B_+(s)a_k^\dagger B_+(0) \rangle = (z_k^* \tilde{N}_k + 2\delta_k^*) \kappa^2 e^{-\phi}, \quad (\text{D23b})$$

$$\langle B_+(s)a_k B_+(0) \rangle = (-z_k N_k + 2\delta_k) \kappa^2 e^{-\phi}, \quad (\text{D23c})$$

$$\langle B_+(s)B_+(0)a_k^\dagger \rangle = \tilde{N}_k z_k^* \kappa^2 e^{-\phi}, \quad (\text{D23d})$$

$$\langle B_+(s)B_+(0)a_k \rangle = -N_k z_k \kappa^2 e^{-\phi}, \quad (\text{D23e})$$

$$\langle B_+(s)a_k^\dagger B_+(0)a_q^\dagger \rangle = \tilde{N}_k z_k^* (\tilde{N}_q z_q^* + 2\delta_q^*) \kappa^2 e^{-\phi}, \quad (\text{D23f})$$

$$\langle B_+(s)a_k B_+(0)a_q \rangle = N_k z_k (N_q z_q - 2\delta_q) \kappa^2 e^{-\phi}, \quad (\text{D23g})$$

$$\langle B_+(s)a_k^\dagger B_+(0)a_q \rangle = [N_k \delta_{kq} - (z_k^* \tilde{N}_k + 2\delta_k^*) N_q z_q] \kappa^2 e^{-\phi}, \quad (\text{D23h})$$

$$\langle B_+(s)a_k B_+(0)a_q^\dagger \rangle = [\tilde{N}_k \delta_{kq} + (-z_k N_k + 2\delta_k) \tilde{N}_q z_q^*] \kappa^2 e^{-\phi}, \quad (\text{D23i})$$

where $z_k \equiv z_k(s)$ is given in Eq. (D19). Substituting Eqs. (D23) into the two-time correlation function and taking the continuum limit one obtains

$$\langle C(s)C(0) \rangle = \kappa^2 e^{-\phi(s)} \left[\Omega_{\mu\mu} \int_0^\infty d\nu J(\nu) (N(\nu) e^{i\nu s} + \tilde{N}(\nu) e^{-i\nu s}) + \sum_{n,m=-1}^1 \tilde{A}_{nm}^{(\cdot,\cdot)}(s) \right]. \quad (\text{D24})$$

Analogously to Eq. (D11), we have defined

$$\tilde{A}_{nm}^{(\cdot,\cdot)}(s) = \int_0^\infty d\nu \int_0^\infty d\nu' A_{nm}^{(\cdot,\cdot)}(\nu, \nu') e^{i\nu s} e^{i\nu' s}, \quad (\text{D25})$$

where written in the matrix notation,

$$A^{(\cdot,\cdot)}(\nu, \nu') = 4 \frac{J(\nu)}{\nu} \frac{J(\nu')}{\nu'} \times \begin{pmatrix} -\Omega_{\mu\Delta} \Omega_{\mu\Delta} \tilde{N}(\nu) \tilde{N}(\nu') & -\Omega_{\mu\Delta} \Omega_{\mu D} \tilde{N}(\nu) & \Omega_{\mu\Delta} \Omega_{\mu\Delta} \tilde{N}(\nu) N(\nu') \\ \Omega_{\mu D} \Omega_{\mu\Delta} \tilde{N}(\nu') & \Omega_{\mu D} \Omega_{\mu D} & -\Omega_{\mu D} \Omega_{\mu\Delta} N(\nu') \\ \Omega_{\mu\Delta} \Omega_{\mu\Delta} N(\nu) \tilde{N}(\nu') & \Omega_{\mu\Delta} \Omega_{\mu D} N(\nu) & -\Omega_{\mu\Delta} \Omega_{\mu\Delta} N(\nu) N(\nu') \end{pmatrix}. \quad (\text{D26})$$

Eq. (D24) is only different from Eq. (D12) due to the position of the four factors of -1 in $A^{(\cdot,\cdot)}(\nu, \nu')$, $\phi(s) \rightarrow -\phi(s)$, and the lack of $\bar{\mu}$ subscripts.

2. Two-time correlation functions $\langle g_\alpha^\dagger(s)g_\beta(0) \rangle$

With the expression for $\langle C^\dagger(s)C(0) \rangle$, $\langle C(s)C^\dagger(0) \rangle$, $\langle C^\dagger(s)C^\dagger(0) \rangle$ and $\langle C(s)C(0) \rangle$ given in Eqs. (D10), (D15), (D20) and (D24) we can now write down the two-time correlation functions $\langle g_\alpha^\dagger(s)g_\beta(0) \rangle$ for $\alpha, \beta \in \{z, +, -\}$. We will write these expressions in the continuum limit using the generic operators

$$g_\alpha = a_\alpha \mathcal{C} + b_\alpha \mathcal{C}^\dagger, \quad (\text{D27})$$

where $\mathcal{C} = C - \kappa V$ and the equivalent for $\alpha \rightarrow \beta$. One can recover the desired two-time correlation functions of g_- , g_+ and g_z by using Table II.

One finds that the two-time correlation functions are

$$\begin{aligned} \langle g_\alpha^\dagger(s)g_\beta(0) \rangle &= -\kappa^2 F_{\alpha\beta} \\ &+ \Gamma_0(s) \kappa^2 \left[(a_\alpha^* a_\beta + b_\alpha^* b_\beta) \Omega_{\mu\bar{\mu}} e^{\phi(s)} + (b_\alpha^* a_\beta \Omega_{\mu\mu} + a_\alpha^* b_\beta \Omega_{\bar{\mu}\bar{\mu}}) e^{-\phi(s)} \right] \\ &+ \kappa^2 \sum_{n,m=-1}^1 \left[(a_\alpha^* a_\beta \tilde{A}_{nm}^{(\cdot,\cdot)}(s) + b_\alpha^* b_\beta \tilde{A}_{nm}^{(\cdot,\dagger)}(s)) e^{\phi(s)} + (b_\alpha^* a_\beta \tilde{A}_{nm}^{(\cdot,\cdot)}(s) + a_\alpha^* b_\beta \tilde{A}_{nm}^{(\dagger,\dagger)}(s)) e^{-\phi(s)} \right], \end{aligned} \quad (\text{D28})$$

α	−	+	z
a_α	$-\sin^2\left(\frac{\varphi}{2}\right)e^{i\theta}$	$\cos^2\left(\frac{\varphi}{2}\right)e^{i\theta}$	$\sin^2\left(\frac{\varphi}{2}\right)\cos^2\left(\frac{\varphi}{2}\right)e^{i\theta}$
b_α	$\cos^2\left(\frac{\varphi}{2}\right)e^{-i\theta}$	$-\sin^2\left(\frac{\varphi}{2}\right)e^{-i\theta}$	$\sin^2\left(\frac{\varphi}{2}\right)\cos^2\left(\frac{\varphi}{2}\right)e^{-i\theta}$

TABLE II. The coefficients used in g_α in Eq. (D27) to obtain the polaron frame coupling operators g_- , g_+ and g_z .

where

$$F_{\alpha\beta} = (a_\alpha^* a_\beta + b_\alpha^* b_\beta) |\langle V \rangle|^2 + b_\alpha^* a_\beta V^2 + a_\alpha^* b_\beta V^*{}^2, \quad (\text{D29})$$

and

$$\Gamma_0(s) = \int_0^\infty d\nu J(\nu) \left[N(\nu)e^{i\nu s} + \tilde{N}(\nu)e^{-i\nu s} \right], \quad (\text{D30})$$

is the correlation function occurring in the standard optical master equation, and all other terms have been previously defined.

The first line of Eq. (D28) arises from the restoring force associated with the non-zero value of $\langle C \rangle = \kappa V$. The second line describes photon emission and absorption with excitation and decay of the dipole, which, for $\phi(s) = 0$, is the term arising in the standard optical master equation scaling as the absolute square of the transition dipole magnitude. For $\phi(s) \neq 0$ there are corrections scaling with $|\mathbf{d}_\Delta|$. The final line in Eq. (D28) describes unique processes due to the strongly coupled permanent dipoles arising from multiphoton processes.

Appendix E: Correlation functions in the displaced frame master equation

If one does not make the polaron transformation of the Hamiltonian in Eq. (9) and instead moves straight to the eigenbasis, one finds the displaced frame Hamiltonian

$$H = \eta^d \tau_z^d + \sum_k \nu_{\mathbf{k}} a_k^\dagger a_k + \sum_{\mu \in \{z, +, -\}} g_{\mu}^d \tau_{\mu}^d, \quad (\text{E1})$$

where $\eta^d = \sqrt{\epsilon'^2 + |V|^2}$ [there is no κ renormalisation of V] and

$$g_z^d = \left[\cos^2 \left(\frac{\varphi^d}{2} \right) - \sin^2 \left(\frac{\varphi^d}{2} \right) \right] A_{\Delta\Delta} + \cos \left(\frac{\varphi^d}{2} \right) \sin \left(\frac{\varphi^d}{2} \right) [e^{i\theta} A_{\mu\bar{\mu}} + e^{-i\theta} A_{\bar{\mu}\mu}] \quad (\text{E2a})$$

$$g_+^d = -2 \cos \left(\frac{\varphi^d}{2} \right) \sin \left(\frac{\varphi^d}{2} \right) A_{\Delta\Delta} + \cos^2 \left(\frac{\varphi^d}{2} \right) e^{i\theta} A_{\mu\bar{\mu}} - \sin^2 \left(\frac{\varphi^d}{2} \right) e^{-i\theta} A_{\bar{\mu}\mu}, \quad (\text{E2b})$$

and $g_-^d = g_+^{d\dagger}$, where

$$A_{pq} = \sum_k (p_k a_k^\dagger + q_k^* a_k). \quad (\text{E3})$$

The Pauli matrices in the eigenbasis are $\tau_{\pm}^d = |\pm^d\rangle \langle \mp^d|$ and $\tau_z^d = |+^d\rangle \langle +^d| - |^-^d\rangle \langle -^d|$ where

$$\begin{pmatrix} |e\rangle \\ |g\rangle \end{pmatrix} = \begin{pmatrix} \cos \left(\frac{\varphi^d}{2} \right) e^{-i\frac{\theta}{2}} & -\sin \left(\frac{\varphi^d}{2} \right) e^{-i\frac{\theta}{2}} \\ \sin \left(\frac{\varphi^d}{2} \right) e^{i\frac{\theta}{2}} & \cos \left(\frac{\varphi^d}{2} \right) e^{i\frac{\theta}{2}} \end{pmatrix} \begin{pmatrix} |+^d\rangle \\ |^-^d\rangle \end{pmatrix}, \quad (\text{E4})$$

with $\cos(\varphi^d) = \epsilon'/\eta^d$, $\sin(\varphi^d) = |V|/\eta^d$ and θ is given in Eq. (26).

Since Eq. (E1) has the same structure as Eq. (13), the master equation in the displaced frame has the same algebraic form as in the polaron frame, i.e. given within the secular approximation by Eqs. (C1) and in full in Appendix C, but the environment correlation functions (ECFs) are different. The displaced frame ECFs depend on linear combinations of Fourier transforms of the form

$$\Gamma_{pq,rs}^d(\omega) = \int_0^\infty ds e^{i\omega s} \langle A_{pq}^\dagger(s) A_{rs}(0) \rangle \equiv \frac{1}{2} \gamma_{pq,rs}^d(\omega) + i S_{pq,rs}^d(\omega). \quad (\text{E5})$$

Substituting Eq. (E3) into the ECF and using that $\langle a_k^\dagger a_{k'} \rangle = \delta_{kk'} N(\nu_{\mathbf{k}})$, $\langle a_k a_{k'}^\dagger \rangle = \delta_{kk'} \tilde{N}(\nu_{\mathbf{k}})$ where $\tilde{N}(\nu) = 1 + N(\nu)$ and that other combinations equal zero, leads to

$$\gamma_{pq,rs}^d(\omega) = 2\pi \left[\Omega_{\bar{p}r} J(\omega) \tilde{N}(\omega) + \Omega_{q\bar{s}} J(-\omega) N(-\omega) \right], \quad (\text{E6a})$$

$$S_{pq,rs}^d(\omega) = \mathcal{P} \int_0^\infty d\nu J(\nu) \left[\Omega_{\bar{p}r} \frac{\tilde{N}(\nu)}{\omega - \nu} + \Omega_{q\bar{s}} \frac{N(\nu)}{\omega + \nu} \right]. \quad (\text{E6b})$$

As usual, an overbar in the subscript denotes the complex conjugate of the dipole vector e.g. $\Omega_{\bar{p}r} = (8\pi/3)(\mathbf{d}_p^* \cdot \mathbf{d}_r)$. Also recall that $J(\omega \leq 0) = 0$ and $\mathbf{d}_{\Delta} \in \Re$.

To exemplify how these functions relate to the rates in Eqs. (C1) we will derive $\gamma_{--}^d(2\eta^d)$ explicitly. This function is given by

$$\gamma_{--}^d(2\eta^d) = 2\Re \int_0^\infty ds e^{2i\eta^d s} \langle g_-^{d\dagger}(s) g_-^d(0) \rangle. \quad (\text{E7})$$

Substituting in g_-^d and using Eqs. (E6) we can read off that [ignoring arguments $(2\eta^d)$ on the right-hand-side and temporarily denoting $\cos(\varphi^d/2) = c$ and $\sin(\varphi^d/2) = s$],

$$\begin{aligned} \gamma_{--}^d(2\eta^d) = & 4c^2 s^2 \gamma_{\Delta\Delta, \Delta\Delta}^d + 2cs^3 e^{i\theta} \gamma_{\Delta\Delta, \mu\bar{\mu}}^d - 2c^3 s e^{-i\theta} \gamma_{\Delta\Delta, \bar{\mu}\mu}^d \\ & + 2cs^3 e^{-i\theta} \gamma_{\mu\bar{\mu}, \Delta\Delta}^d + s^4 \gamma_{\mu\bar{\mu}, \mu\bar{\mu}}^d - s^2 c^2 e^{-2i\theta} \gamma_{\mu\bar{\mu}, \bar{\mu}\mu}^d \\ & - 2c^3 s e^{i\theta} \gamma_{\bar{\mu}\mu, \Delta\Delta}^d - c^2 s^2 e^{2i\theta} \gamma_{\bar{\mu}\mu, \mu\bar{\mu}}^d + c^4 \gamma_{\bar{\mu}\mu, \bar{\mu}\mu}^d. \end{aligned} \quad (\text{E8})$$

Using the symmetry that $\Omega_{ab} = \Omega_{ba}$ and that $\mathbf{d}_\Delta \in \Re$, we can read off from Eq. (E6a) that

$$\gamma_{\Delta\Delta,\Delta\Delta}^d(2\eta^d) = \Omega_{\Delta\Delta}\gamma_0(2\eta^d), \quad (\text{E9})$$

$$\gamma_{\bar{\mu}\mu,\mu\bar{\mu}}^d(2\eta^d) = \Omega_{\mu\mu}\gamma_0(2\eta^d), \quad (\text{E10})$$

$$\gamma_{\mu\bar{\mu},\bar{\mu}\mu}^d(2\eta^d) = \Omega_{\bar{\mu}\bar{\mu}}\gamma_0(2\eta^d), \quad (\text{E11})$$

$$\gamma_{\bar{\mu}\mu,\Delta\Delta}^d(2\eta^d) = \gamma_{\Delta\Delta,\mu\bar{\mu}}^d(2\eta^d) = \Omega_{\mu\Delta}\gamma_0(2\eta^d), \quad (\text{E12})$$

$$\gamma_{\mu\bar{\mu},\Delta\Delta}^d(2\eta^d) = \gamma_{\Delta\Delta,\bar{\mu}\mu}^d(2\eta^d) = \Omega_{\bar{\mu}\Delta}\gamma_0(2\eta^d), \quad (\text{E13})$$

$$\gamma_{\mu\bar{\mu},\mu\bar{\mu}}^d(2\eta^d) = \gamma_{\bar{\mu}\mu,\bar{\mu}\mu}^d(2\eta^d) = \Omega_{\mu\bar{\mu}}\gamma_0(2\eta^d), \quad (\text{E14})$$

where $\gamma_0(\omega) = 2\pi[J(\omega)\tilde{N}(\omega) + J(-\omega)N(-\omega)]$. Using these we find that

$$\gamma_{--}^d(2\eta^d) = k_{--}^0\gamma_0(2\eta^d), \quad (\text{E15})$$

where the rate coefficient is

$$k_{--}^0 = [c^4 + s^4]\Omega_{\mu\bar{\mu}} + 4c^2s^2\Omega_{\Delta\Delta} - s^2c^2[e^{-2i\theta}\Omega_{\bar{\mu}\bar{\mu}} + e^{2i\theta}\Omega_{\mu\mu}] - 2sc[c^2 - s^2][e^{-i\theta}\Omega_{\bar{\mu}\Delta} + e^{i\theta}\Omega_{\mu\Delta}]. \quad (\text{E16})$$

This is rather complicated but only because we have complex transition dipole elements. If we assume real transition dipoles [$\mathbf{d}_{\bar{\mu}} \rightarrow \mathbf{d}_\mu$ and $\theta \rightarrow 0$] we find $k_{--}^0 = \Omega_{--}$ where we have defined a new dipole vector

$$\mathbf{d}_- = [c^2 - s^2]\Re[\mathbf{d}_\mu] + 2cs\mathbf{d}_\Delta. \quad (\text{E17})$$

Likewise, if we choose purely imaginary transition dipoles [$\mathbf{d}_\mu \rightarrow i\Im[\mathbf{d}_\mu]$, $\mathbf{d}_{\bar{\mu}} \rightarrow -i\Im[\mathbf{d}_\mu]$ and $\theta \rightarrow \pi/2$] we find that $k_{--}^0 = \Omega_{--}$ but with the dipole vector now defined as

$$\mathbf{d}_- = [c^2 - s^2]\Im[\mathbf{d}_\mu] + 2cs\mathbf{d}_\Delta. \quad (\text{E18})$$

A final limit worth checking is when the eigenstates fully localise, $|+\rangle \rightarrow |e\rangle$ and $|-\rangle \rightarrow |g\rangle$, i.e. $c \rightarrow 1$ and $s \rightarrow 0$. In this case, $k_{--}^0 \rightarrow \Omega_{\mu\bar{\mu}}$, and so the decay rate is $\gamma_{--}^d(2\eta^d) = \gamma_{--}^d(2\epsilon') = \Omega_{\mu\bar{\mu}}\gamma_0(2\epsilon')$, which is the standard decay rate in the optical master equation.

Appendix F: Polaron rates for larger $|\mathbf{d}_D|$

In this appendix we show in Fig. 7 how the decay, excitation and decoherence rates depend on $|\mathbf{d}_\Delta|$ for increasingly large $|\mathbf{d}_D|$. One can see that, for small and even moderately large values of $|\mathbf{d}_D|$, the dependence of the *normalised* rates on $|\mathbf{d}_\Delta|$ are identical. Only when $|\mathbf{d}_D| \sim 2 \text{ eV}^{-1}$ does the dependence of the excitation rate on \mathbf{d}_Δ differ noticeably from the other two rates. For all parameters here, we also find that $\gamma_d \approx (\gamma_\downarrow + \gamma_\uparrow)/2$ is a good approximation, meaning that the pure dephasing term in Eq. (31) is negligible.

We will now give the maximum values of each rate for each subfigure of Fig. 7 in the format, $\{\text{Max}(\gamma_\downarrow), \text{Max}(\gamma_\uparrow), \text{Max}(\gamma_d)\}$:

- $|\mathbf{d}_D| = 0 \text{ eV}^{-1}$: $\{1.083, 0.147, 0.615\} \text{ ps}^{-1}$;
- $|\mathbf{d}_D| = 0.2 \text{ eV}^{-1}$: $\{2.472, 0.334, 1.403\} \text{ ps}^{-1}$;
- $|\mathbf{d}_D| = 0.5 \text{ eV}^{-1}$: $\{7.556, 1.018, 4.287\} \text{ ps}^{-1}$;
- $|\mathbf{d}_D| = 1 \text{ eV}^{-1}$: $\{22.89, 3.061, 12.98\} \text{ ps}^{-1}$;
- $|\mathbf{d}_D| = 2 \text{ eV}^{-1}$: $\{78.48, 10.19, 44.33\} \text{ ps}^{-1}$;
- $|\mathbf{d}_D| = 5 \text{ eV}^{-1}$: $\{423.4, 47.95, 236.1\} \text{ ps}^{-1}$.

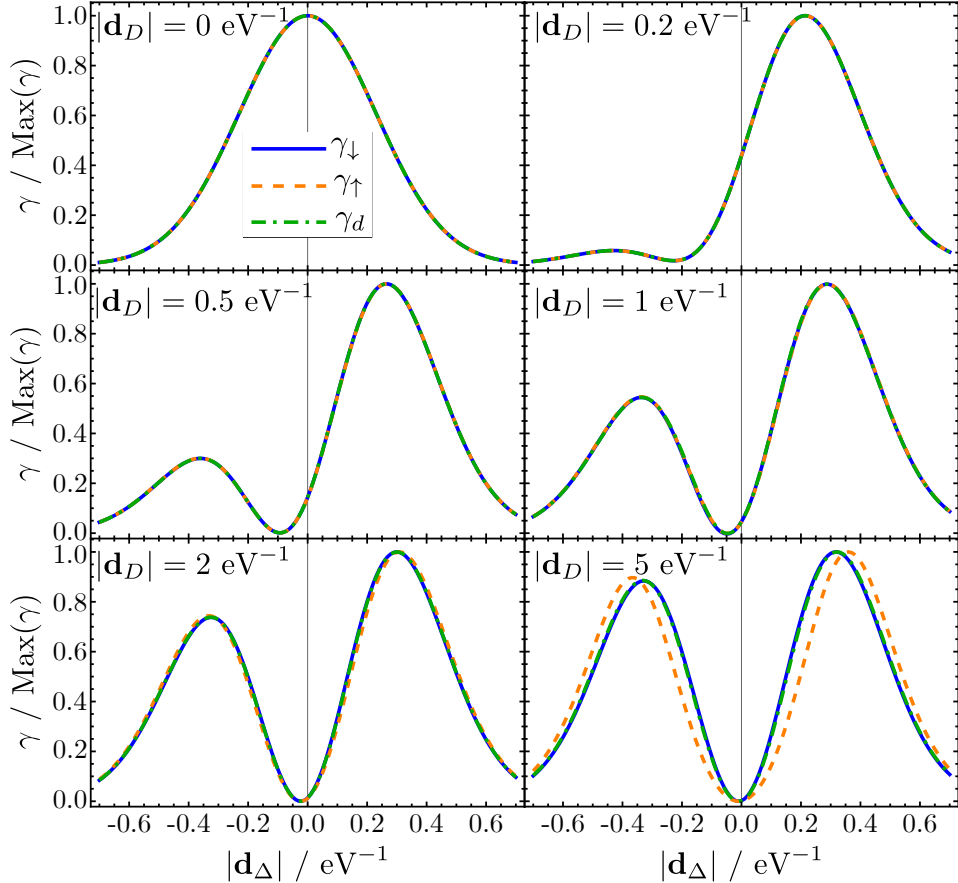


FIG. 7. **Normalised polaron frame decay, excitation and decoherence rates for different permanent dipole strengths.** The parameters used in this figure are the same as in Fig. 3 unless specified within this figure. Recall that all dipole vectors \mathbf{d}_μ , \mathbf{d}_D and \mathbf{d}_Δ are co-linear.

Appendix G: Derivation of the emission spectrum

In this appendix, we derive Eq. (49), which gives the emission spectrum for the single emitter system. Our derivation closely follows those provided for single emitter systems without permanent dipoles in Refs. [2, 65–68]. Due to the permanent dipoles, there are additional light-matter interaction terms in the Hamiltonian in Eq. (4), and so the derivation is slightly more cumbersome. However, as we show here, these additional terms do not affect the expression for the emission spectrum of the emitter.

The emission spectrum is given exactly by

$$I(\omega) = \lim_{t \rightarrow \infty} \Re \int_0^\infty d\tau e^{i\omega\tau} \langle \mathbf{E}_-(\mathbf{R}, t) \cdot \mathbf{E}_+(\mathbf{R}, t + \tau) \rangle, \quad (\text{G1})$$

where \mathbf{R} is the position of the detector and the positive frequency component of the electric field is

$$\mathbf{E}_+(\mathbf{R}, t) = i \sum_k \mathbf{e}_k f_k a_k e^{-i\mathbf{k} \cdot \mathbf{R}}, \quad (\text{G2})$$

and $\mathbf{E}_-(\mathbf{R}, t) = \mathbf{E}_+(\mathbf{R}, t)^\dagger$. Our aim is to express the expectation value $\langle a_k^\dagger a_q \rangle$ in terms of dipole operators σ_\pm , which is achieved through the Heisenberg equation of motion

$$\frac{\partial}{\partial t} a_k(t) = -i [H, a_k(t)], \quad (\text{G3})$$

where H is the lab frame Hamiltonian in Eq. (1) and equivalently in Eq. (4). In doing so we will have arrived at the form of the emission spectrum in Eq. (49).

Using $[a_k, a_q^\dagger] = \delta_{kq}$, one can show that

$$\frac{\partial}{\partial t} a_k(t) = -i\nu_k a_k(t) - \Delta_k \sigma_z(t) - \mu_k \sigma_+(t) - \mu_k^* \sigma_-(t), \quad (\text{G4})$$

where $\sigma_\alpha(t) = U(t)^\dagger \sigma_\alpha U(t)$ and $U(t) = \exp(-iHt)$, which can be solved to yield

$$a_k(t) = a_k(0) e^{-i\nu_k t} - \int_0^t d\tau e^{i\nu_k(\tau-t)} [\Delta_k \sigma_z(\tau) + \mu_k \sigma_+(\tau) - \mu_k^* \sigma_-(\tau)]. \quad (\text{G5})$$

The first term in Eq. (G5) is the free field term which does not contribute to the spectrum of the emitter and is henceforth ignored. After substituting the second term of Eq. (G5) into Eq. (G2) and taking the continuum limit we obtain

$$\mathbf{E}_+(\mathbf{R}, t) = \int_0^\infty d\nu \sqrt{J(\nu)} \int_0^t d\tau e^{i\nu_k(\tau-t)} [\mathbf{O}_z \sigma_z(\tau) + \mathbf{O}_\mu \sigma_+(\tau) + \mathbf{O}_{\bar{\mu}} \sigma_-(\tau)], \quad (\text{G6})$$

where

$$\mathbf{O}_p = \int_{d\Omega_k} d\Omega_k \sum_\lambda \mathbf{e}_k (\mathbf{d}_p \cdot \mathbf{e}_k) e^{i\mathbf{k} \cdot (\mathbf{r} - \mathbf{R})}. \quad (\text{G7})$$

To progress analytically, we need to know how the emitter operators $\sigma_\alpha(t)$ evolve in time. However, this is very complicated. Instead, we make the so-called harmonic decomposition (see Chapter 2.2 of Ref. [2]) in which we assume that the timescale over which the emitter evolves unitarily is much faster than the timescale over which spontaneous emission occurs. Within this approximation, we write that

$$\sigma_+(t) \approx \sigma_+(t) e^{i\omega_0(\tau-t)}, \quad \sigma_-(t) \approx \sigma_-(t) e^{-i\omega_0(\tau-t)}, \quad \text{and, } \sigma_z(t) \approx \sigma_z(t), \quad (\text{G8})$$

where $\omega_0 = 2\epsilon$ is the emitter energy splitting. Making the harmonic decomposition in Eq. (G6) yields

$$\mathbf{E}_+(\mathbf{R}, t) = \int_0^\infty d\nu \sqrt{J(\nu)} [\mathbf{O}_z \sigma_z(t) j_0(\nu, t) + \mathbf{O}_\mu \sigma_+(t) j_+(\nu, t) + \mathbf{O}_{\bar{\mu}} \sigma_-(t) j_-(\nu, t)], \quad (\text{G9})$$

where

$$j_\alpha(\nu, t) = \int_0^t d\tau e^{i(\tau-t)(\nu + \alpha\omega_0)} = -i \frac{1 - e^{-it(\nu + \alpha\omega_0)}}{\nu + \alpha\omega_0}. \quad (\text{G10})$$

The function $j_\alpha(\nu, t)$ is dominated by the contribution near to $\nu = -\alpha\omega_0$ and so we approximate it as a delta function, $j_\alpha(\nu, t) \approx 2\pi\delta(\nu + \alpha\omega_0)$ [2]. After performing this approximation, one finds that the delta function corresponding to $j_+(\nu, t)$ lies outwith the integration domain $\nu \in [0, \infty]$ and so the term going as $\sigma_+(t)$ in Eq. (G9) vanishes. Moreover, the term proportional to $j_0(\nu, t)$ provides a delta function at zero frequency, leading to the term going as $\sigma_z(t)$ in Eq. (G9) to be proportional to $\sqrt{J(0)}$. This is equal to zero for any well-defined spectral density. Therefore, within the standard approximations outlined in this derivation, the presence of permanent dipoles does not change the expression of the emission spectrum from Eq. (49). Thus, the only surviving term in Eq. (G9) is proportional to $\sigma_-(t)$, and so we obtain

$$\mathbf{E}_+(\mathbf{R}, t) \approx 2\pi\sqrt{J(\omega_0)}\mathbf{O}_{\bar{\mu}}(\mathbf{r}, \mathbf{R})\sigma_-(t), \quad (\text{G11})$$

where we have made the dependence of $\mathbf{O}_{\bar{\mu}}$ on \mathbf{r} and \mathbf{R} explicit. After substituting Eq. (G11) and its Hermitian conjugate into Eq. (G1), one obtains Eq. (49).

Appendix H: Effective Hamiltonian

In many numerical schemes to solve the open quantum dynamics of systems coupled to thermal environments, it is assumed that the environment is in a free Gibbs state at the associated temperature $T = 1/\beta$. In the polaron framework, the environment is not in such a convenient form. As such, we derive here an effective Hamiltonian that encapsulates the polaron thermalised state but has the effective environment in a free Gibbs state.

We start with the lab frame Hamiltonian,

$$H = \epsilon \sigma_z + \sum_k \nu_{\mathbf{k}} a_k^\dagger a_k + A_{DD} \mathcal{I} + A_{\Delta\Delta} \sigma_z + A_{\mu\bar{\mu}} \sigma_+ + A_{\bar{\mu}\mu} \sigma_-, \quad (\text{H1})$$

where

$$A_{pq} = \sum_k (p_k a_k^\dagger + q_k^* a_k), \quad (\text{H2})$$

$$p_k = i f_{\mathbf{k}} e^{i \mathbf{k} \cdot \mathbf{r}} (\mathbf{d}_p \cdot \mathbf{e}_{\mathbf{k}}), \quad (\text{H3})$$

with $p, q \in \{\mu, \bar{\mu}, D, \Delta\}$, with an initial state which is a displaced thermal environment state.

In our calculations, the polaron frame initial state is

$$\rho_p^0 = |g\rangle \langle g| \otimes \rho_E, \quad (\text{H4})$$

where $\rho_E = \exp[-\beta \sum_k \nu_{\mathbf{k}} a_k^\dagger a_k]/\mathcal{Z}_E$ is a thermal state. Perform the inversion of the unitary transformations to go from the displaced polaron frame to the displaced frame, the initial state is $\rho_d^0 = U^\dagger \rho_p^0 U$ where the polaron transformation is $U = B(\delta) |e\rangle \langle e| + B(-\delta) |g\rangle \langle g|$ and $\delta_k = \Delta_k/\nu_{\mathbf{k}}$ and $B(\alpha) = \exp[\sum_k (\alpha_k a_k^\dagger - \alpha_k^* a_k)]$. Therefore,

$$\rho_d^0 = |g\rangle \langle g| \otimes \eta(\delta), \quad (\text{H5})$$

where we have defined a displaced thermal state as $\eta(\alpha) = B(\alpha) \rho_E B(-\alpha)$. We can then obtain the lab frame initial state via $\rho^0 = B(-d) \rho_d^0 B(d)$ where $d_k = D_k/\nu_{\mathbf{k}}$, leading to

$$\rho^0 = |g\rangle \langle g| \otimes \eta(\delta - d). \quad (\text{H6})$$

The expression for $\eta(\alpha)$ can be rewritten by making use of the identity:

$$\exp(e^S X e^{-S}) = e^S e^X e^{-S}, \quad (\text{H7})$$

which holds if $e^S e^{-S} = \mathcal{I}$. Using this identity we can write,

$$\eta(\alpha) = \exp \left[-\beta \sum_k \nu_{\mathbf{k}} (a_k^\dagger - \alpha_k^*) (a_k - \alpha_k) \right]. \quad (\text{H8})$$

Let's rewrite the lab frame Hamiltonian using new ladder operators b_k , which we will now relate to the a_k to ensure we model our desired initial state, $\eta(\delta - d)$. The initial environment state in the effective lab frame will be $\bar{\rho}_E = \exp[-\beta \sum_k \nu_{\mathbf{k}} b_k^\dagger b_k]/\mathcal{Z}_E$ and so by comparison with Eq. (H8), we know that

$$b_k = a_k - (\delta_k - d_k). \quad (\text{H9})$$

Substituting this into our actual lab frame Hamiltonian in Eq. (H1) and ignoring any terms that are identity operators in both Hilbert spaces, we arrive at the effective Hamiltonian:

$$\bar{H} = \bar{H}_0 + \bar{H}_I, \quad (\text{H10})$$

where

$$\bar{H}_0 = (\epsilon + \chi_{\Delta\Delta}) \sigma_z + \chi_{\mu\bar{\mu}} \sigma_+ + \chi_{\bar{\mu}\mu} \sigma_- + \sum_k \nu_{\mathbf{k}} b_k^\dagger b_k, \quad (\text{H11})$$

$$\bar{H}_I = B_{\Delta\Delta} (\mathcal{I} + \sigma^z) + B_{\mu\bar{\mu}} \sigma_+ + B_{\bar{\mu}\mu} \sigma_-, \quad (\text{H12})$$

where

$$B_{pq} = \sum_k (p_k b_k^\dagger + q_k^* b_k), \quad (\text{H13})$$

$$\chi_{pq} = \sum_k (p_k h_k^* + q_k^* h_k), \quad (\text{H14})$$

$$h_k = \delta_k - d_k. \quad (\text{H15})$$

In order to get numerical agreement between TEMPO and the PFME, both of which assume separable initial states but crucially in different frames, we, therefore, must use \bar{H} in Eq. (H10) for TEMPO calculations.